Results in Optics 3 (2021) 100073

Contents lists available at ScienceDirect

Results in Optics

journal homepage: www.elsevier.com/locate/rio

Enhanced Photoluminescence with Dielectric Nanostructures: A review

Hiba Alhalaby [a,b,*], Haitham Zaraket [a], Maria Principe [b,*]

[a] Multi-Disciplinary Physics Laboratory, Optics and Fiber Optics Group, Faculty of Sciences, Lebanese University, Hadath 1003, Lebanon
[b] Optoelectronics Group, Department of Engineering, University of Sannio, Benevento 82100, Italy

ARTICLE INFO

Keywords:
Resonant dielectric nanostructures
Photoluminescence enhancement
Mie theory

ABSTRACT

Resonant dielectric subwavelength structures made of high-refractive-index materials are an emerging powerful platform with unique advantages compared to plasmonic based nanostructures. Owing to the low ohmic losses, to their ability to localize optical near-field at nanoscale, and exciting both electric and magnetic resonant modes, high-index dielectric materials are being used in various applications. Starting from the first principles, we aim at showing how resonant dielectric nanostructures can be efficiently used to enhance photoluminescence signal from an excited molecule, and we review the most recent results present in the Literature.

1. Introduction

Photoluminescence (PL) is the spontaneous emission of light from a material following optical excitation. PL can be divided into two categories: fluorescence and phosphorescence, depending mainly upon the configuration of the electronic excited state and its lifetime (Lichtman and Conchello, 2005).

Analysis of the PL activity of a given material, named as Photoluminescence Spectroscopy (Lakowicz, 2006), is a powerful technique to probe the internal structure of a molecule, in order to extract valuable information about sample composition. Indeed, PL is widely used in biochemistry and molecular biology (Molinari, 2015) to characterize complex molecules, their environment, or their location, it is also used to characterize the optoelectronic properties of semiconductors (Perkowitz, 2012).

Alternatively, knowing the properties of a given molecule, its PL activity can be used to detect the presence of a relevant target analyte in a solution. This is how fluorescence is being used in biological experiments: a fluorochrome or dye is allowed to bind to a specific target molecule, e.g. a protein biomarker (Yu et al., 2004; Mukundan et al., 2009), acting as a "label", so that the target molecule can be detected by fluorescence analysis.

In these kinds of experiments, it can be also very important to determine the concentration of the target molecule, for example, for diagnosis and choice of medical treatment. Target concentration is indirectly measured via the concentration of dyes (Yu et al., 2004; Mukundan et al., 2009). However, the concentration of many clinically relevant targets can reach very low values, e.g. some biomarkers reside in human blood at picomolar concentrations or lower.

Hence, one of the most important topics of research in the field of biological and chemical sensing, on which researchers have been very active in recent years, is to enhance the PL signal to improve the sensitivity of detection in order to detect very low concentrations of the target analyte. Among the main directions explored to enhance the PL signal, there are: i) the optimization of the design of the photoluminescent particle, e.g. a fluorochrome bound to a larger molecule (Resch-Genger et al., 2008); ii) the improvement of the detection methods and apparatus (Barnes et al., 1993; Eigen and Rigler, 1994); iii) the design of optimized substrates able to amplify the PL signal (Hung et al., 2006; Lu et al., 2012; Geddes and Lakowicz, 2002; Ganesh et al., 2007; Dorfman et al., 2006; Zhao et al., 2008; Gu et al., 2008; Goldys et al., 2007; Li et al., 2011).

With reference to this last direction, several plasmonic substrates have been proposed throughout the years (Laux et al., 2017; Koenderink, 2017), given their great ability to amplify an impinging electric field.

However, plasmonic materials suffer from high dissipation losses causing heat generation in the structure which can be a limitation in many applications. Besides, owing to the high absorbance of metals, a quantum emitter positioned in the vicinity of a plasmonic nanostructure undergoes quenching, which makes dielectric spacers essential between the emitter and the nanostructure, compromising the field enhancement near the nanostructure. To overcome these limitations, dielectric materials have been lately introduced. In addition to its

* Corresponding authors at: Optoelectronics Group,Department of Engineering, University of Sannio, Benevento 82100, Italy (H. Alhalaby and M. Principe).
E-mail addresses: hiba.alhalaby@unisannio.it (H. Alhalaby), principe@unissanio.it (M. Principe).

https://doi.org/10.1016/j.rio.2021.100073
Received 25 January 2021; Revised 25 January 2021; Accepted 11 February 2021
Available online xxxx

reduced absorption, it has been theoretically demonstrated (Evlyukhin et al., 2010; García-Etxarri et al., 2011) and experimentally verified (Evlyukhin et al., 2012; Kuznetsov et al., 2012) that nanoparticles of high refractive index dielectric materials, support both electric and magnetic multipolar Mie-resonances in the visible and near-infrared range. In particular, these properties triggered researchers' interest to develop resonant nanostructures based on high-index dielectric materials. Indeed, resonant dielectric nanostructures have been used for different applications. In this article, we focus on the recent development of high-index dielectric nanostructures for PL enhancement. Section 2 gives the fundamental principles of PL. Section 3 summarizes the Mie theory that explains the scattering of light by simple resonant dielectric nanostructures. Section 4 provides a brief explanation of the key factors for enhancing the luminescence of an emitter coupled to the optical resonator. We describe the spontaneous emission enhancement explaining the strong and weak coupling regimes and Purcell effect, in addition to controlling the directivity through an engineered interference of the electric and magnetic multipole Mie resonance. Finally, recent developments in PL enhancement based on high-index dielectric nanostructures achieved so far are reviewed in Section 5.

2. Photoluminescence in a nutshell

To illustrate the process yielding PL, Fig. 1 shows a simplified Jablonski diagram, where S_0 and S_1 represent the lowest-energy electronic states (singlet ground state, first and second singlet states, respectively), and T_1 represents a triple excited state (Lakowicz, 2006). In each state there are several energy levels, depicted as thinner horizontal lines, corresponding to different vibrational and/or rotational states.

With ultraviolet or visible light, common photoluminescent molecules are usually excited to higher vibrational levels of the first or second singlet energy state. Irradiation with a wide spectrum of wavelengths will generate an entire range of allowed transitions that populate the vibrational energy levels of excited states: some of these transitions have a higher probability than others to occur, thus yielding the absorption spectrum of the molecule.

Following the absorption of a photon, several processes of relaxation occur with different probabilities, and on the relaxation pathway depends whether a photon is emitted (radiative relaxation) or not (non-radiative relaxation), and whether it is a fluorescence or a phosphorescence process.

The first most likely transition is toward the lowest vibrational energy level of the excited state through an internal conversion process, which typically occurs within a few picoseconds or less, and entails some loss of energy without emission of light. Thus, the excited

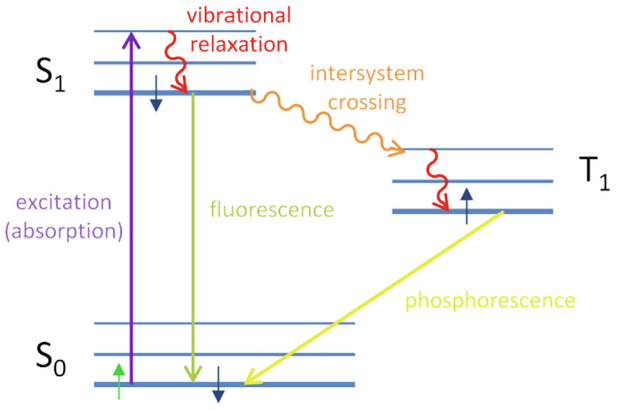

Fig. 1. Simplified Jablonksy diagram showing internal PL processes (Lakowicz, 2006).

molecule in the lowest level of the excited singlet state exists for a period of time, before relaxing to the ground state. When fluorescence takes place, such relation is accompanied by the emission of a photon. The closely spaced vibrational and rotational levels of the ground state determine an emission intensity over a band of wavelengths.

In view of the partial loss of energy during the decay to the lowest vibrational energy level of the excited state, the energy associated with the emitted photon during the fluorescence process is typically less than the energy associated with the absorbed photon, and hence the emitted light has longer wavelengths than the absorbed light. This phenomenon is generally known as Stokes shift and can vary from few nanometers to several hundreds of nanometers depending on the molecular structures (e.g. it is about 20 nm for fluorescein and 110 nm for quinine).

In view of the described process, the main characteristics of a fluorochrome are the intrinsic quantum yield η_0 and the lifetime τ_0. The intrinsic quantum yield η_0 is the probability to emit a photon after absorption, or in other terms, it is the number of emitted photons over the number of absorbed photons. It is defined as $\eta_0 = \frac{\gamma_{mol}^{0,rad}}{\gamma_{mol}^{0}}$,

where $\gamma_{mol}^{0} = \gamma_{mol}^{0,rad} + \gamma_{mol}^{0,loss}$ is molecule decay rate in free space and $\gamma_{mol}^{0,rad}$ and $\gamma_{mol}^{0,loss}$ are the radiative and non-radiative decay rates of the molecule, respectively, which depend upon its electronic structure defining the probabilities of the state transitions.

The lifetime τ_0 is defined as the average time the molecule takes to relax to the ground state from the excited state, and it is of the order of tens of nanoseconds for fluorescence. The longer τ_0 the higher the probability that the molecule reacts with the surrounding environment, such as with oxygen-free radicals, causing photobleaching. Hence it is desirable for the fluorophore to have a short lifetime, yielding a good photostability. The lifetime is related to the radiative and non-radiative decay rate by the equation

$$\tau_0 = \frac{1}{\gamma_{mol}^{0,rad} + \gamma_{mol}^{0,loss}} = \frac{\eta_0}{\gamma_{mol}^{0,rad}}.$$

From the experimental point of view, it is desirable to have a high quantum yield, yielding, in the same experimental conditions, a higher detectable photoluminescent signal with respect to a molecule with low quantum yield.

Enhancing the intrinsic value of η_0 of a given molecule is hard since, as stated before, it depends on its internal electronic state transitions. However, in view of the oscillating dipole behavior of an excited photoluminescent particle (Malicka et al., 2003; Gerber et al., 2007), internal processes can be affected by a coupled resonant cavity that modifies the local electromagnetic environment.

How this can be done with a resonant cavity of dielectric material, is summarized in the following sections, and the most recent results in the pertinent literature are reviewed.

3. Optical response from a single particle: Mie theory

When a particle is illuminated by an incident monochromatic wave (E_i, H_i), as shown in Fig. 2, the electric field around the particle (E) is given by the superposition between the incident (E_i) and the scattered field (E_s). The total Poynting vector $(\vec{S} = \frac{1}{2} Re\left[\vec{E}_{tot} \times \vec{H}^{*}_{tot}\right])$ will then be the sum of the incident Poynting vector S_i, the scattering Poynting vector S_s and the interference or extinction part S_{ext}

$$\vec{S} = \vec{S}_i + \vec{S}_s + \vec{S}_{ext}. \quad (1)$$

Define a volume V enclosing the scattering object, and ∂V its surface (Fig. 2). Since the host medium is assumed to be non-dissipative, the net average rate at which the electromagnetic energy crosses the closed boundary ∂V of the volume is always nonnegative and is equal to the power absorbed by the object, yielding

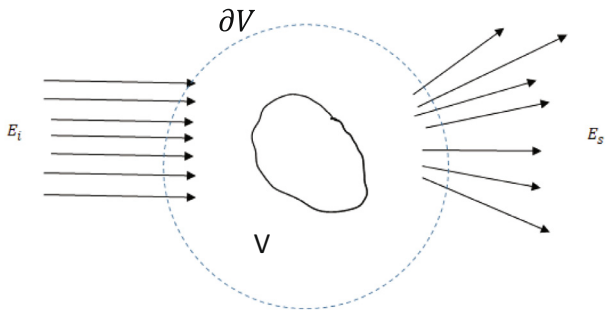

Fig. 2. Scattering of an arbitrary particle with the incident wave from left having an electric field E_i and scattered field E_s. The dashed sphere is a control surface used to evaluate the total energy flux.

$$P_{abs} = -\iint d\vec{A}\cdot\vec{S} = -\iint d\vec{A}\cdot\vec{S}_{ext} - \iint d\vec{A}\cdot\vec{S}_s \equiv P_{ext} - P_{scat} \tag{2}$$

where the contribution of S_i vanished being the surrounding medium non-dissipative and we used the sign convention taken to give a positive power for the absorbed power (P_{abs}), the extinction power (P_{ext}), and the scattering power (P_{scat}) (an outgoing wave from the nanoparticle).

The internal and external fields of the particle are obtained by solving Maxwell's equation, with the pertinent boundary conditions, with the aid of numerical methods such as finite-difference time-domain (Sevgi, 2014) or finite-element method (Jin, 2015). Indeed, complex shapes and/or multimer antennas are considered to engineer the scattered field distribution and strength, by properly tuning the geometrical dimensions. To narrow the optimization parameter space, it would be useful to have some benchmark structures, e.g. a spherical particle, for which the problem can be solved analytically. Mie theory is the canonical frame for studying the scattering of spherical particles. In what follows we will review the main points of Mie theory.

Mie theory, which was developed by Gustav Mie in 1908 (Mie, 1908), has been adopted for the study of the scattering and absorption of plane electromagnetic waves by small isotropic particles (Hergert, 2012). As reported in Mie theory (Bohren, 1983), spherical particles can seize strong scattering resonance regardless of their material type. In fact, the scattering properties of lossless and nonmagnetic materials are governed mainly by two variables that are the dielectric permittivity ε and the size parameter q, which is proportional to the radius R and the wavelength of light λ defined as $q = \frac{2\pi R}{\lambda} \equiv kR$.

The spherical symmetry of the particle, biased by the incident field propagation direction, leads to a normal mode decomposition given by Bessel functions and Modified Legendre polynomials. The latter functions have a clear link interpretation that was encountered in electrostatics and magneto-static: the electric and magnetic multipole expansion.

For a spherical particle, it is useful to define the dimensionless quantity called the efficiency $Q = P/\pi R^2 I_i$, where the normalization is made with respect to the incident wave intensity and that of the projected area of the sphere (πR^2). The scattering (Q_{sct}), absorption (Q_{abs}) and extinction (Q_{ext}) efficiencies can be obtained from the Mie theory as:

$$\begin{aligned} Q_{sct} &= \tfrac{2}{(kR)^2}\textstyle\sum_{j=1}^{\infty}(2j+1)(|a_j|^2 + |b_j|^2) \\ Q_{ext} &= \tfrac{2}{(kR)^2}\textstyle\sum_{j=1}^{\infty}(2j+1)\mathrm{Re}(|a_j| + |b_j|) \\ Q_{abs} &= Q_{ext} - Q_{sct} \end{aligned} \tag{3}$$

where the coefficients a_j and b_j are the electric and magnetic Mie scattering amplitudes, $k = \frac{2\pi n}{\lambda} = \frac{\omega n}{c}$ is the wavenumber, c is the speed of light and n is the refractive index of the medium. Usually, a finite set of multipoles are needed. For example a_1 and b_1, which denote the electric and magnetic dipole modes, will dominate when the incident wavelength is much greater than the diameter of the nanoparticle.

The electric and magnetic scattering amplitudes are defined as:

$$a_j = \frac{R_j^{(a)}}{R_j^{(a)} + iT_j^{(a)}}, b_j = \frac{R_j^{(b)}}{R_j^{(b)} + iT_j^{(b)}} \tag{4}$$

where R_j and T_j can be expressed as

$$\begin{aligned} R_j^{(a)} &= n\psi_j'(kR)\psi_j(nkR) - \psi_j'(nkR)\psi_j(kR) \\ T_j^{(a)} &= n\chi_j'(kR)\psi_j(nkR) - \psi_j'(nkR)\chi_j(kR) \\ R_j^{(b)} &= n\psi_j'(nkR)\psi_j(kR) - \psi_j'(kR)\psi_j(nkR) \\ T_j^{(b)} &= n\chi_j(kR)\psi_j'(nkR) - \psi_j(nkR)\chi'_j(kR) \end{aligned} \tag{5}$$

here, $\psi_j(x) = \sqrt{\frac{\pi x}{2}}J_{j+\frac{1}{2}}(x), \chi_j(x) = \sqrt{\frac{\pi x}{2}}N_{j+\frac{1}{2}}(x)$, $J_{j+\frac{1}{2}}(x)$ and $N_{j+\frac{1}{2}}(x)$ are the Bessel and Neumann functions, with the prime representing derivatives (Bohren and Huffman, 1998).

The resonant enhancement of scattering and extinction cross-section spectra is determined by the equations $R_j^{(a)} + iT_j^{(a)} = 0$ and $R_j^{(b)} + iT_j^{(b)} = 0$ of the electric and magnetic eigenmodes respectively. In the general case, these expressions are fulfilled at complex frequencies $\omega_j = Re[\omega_j] + iIm[\omega_j]$. Due to the flow of energy outside the particle and its depletion into absorption, a mode has a finite lifetime $1/\gamma_c = 2Im[\omega_j]$ where γ_c is defined as the cavity decay rate, which determines the half-width of the resonance line at half maximum (Sauvan et al., 2013). The quality factor (not to be confused with the efficiency defined before) denoted by $Q = \frac{\omega}{\gamma_c}$ characterizes the resonance. Both radiative and absorptive parts are comprised in the cavity decay rate $\gamma_c = \gamma_c^{rad} + \gamma_c^{loss}$, such that the quality factor can be denoted as $Q^{-1} = Q_{rad}^{-1} + Q_{loss}^{-1}$ (Bliokh et al., 2008).

The contribution from each multipole (Electric or Magnetic) can be seen as a resonant (ripple) structure in the scattering cross-section. In Fig. 3(a) we consider a Si sphere of radius 75 nm, the dispersive behavior of the sphere was taken into consideration using the data from (Aspnes and Studna, 1983). One can identify the electric dipole behavior near 500 nm and then the Magnetic dipole around 615 nm. Losses are higher for electric dipole than the magnetic dipole, partially due to the difference in the value of the extinction coefficient. The contribution from higher multipoles can also be noticed. We can further illustrate the ripple structure due to the multipole expansion by considering a theoretical dielectric sphere without dispersion as shown in Fig. 3(b). The electric and magnetic field maps are for electric and magnetic dipole resonance in Fig. 3(c) illustrating that the magnetic field can be enhanced inside the dielectric sphere at magnetic dipole resonance.

In short, due to the field penetration and phase retardation within the particle, the resonant magnetic dipole reaction occurs from a coupling of the incident wave to the radial displacement currents of the electric field. This happens when the wavelength inside the particle is close to the diameter of the particle $2R \approx \lambda/n$. In the considered case $2R = 150$ nm and $n \approx 4$ (in the region of interest) hence the resonance is around 600 nm.

Krasnok et al. (Krasnok et al., 2018) compared the scattering and absorption cross-sections of metallic (Silver Ag) nanoparticle (NP) and high index dielectric NP made of crystalline (c-Si). The results show that Ag NP comprises electric type multipole resonance whose dispersion is shown with increasing radius in Fig. 4(a). Their magnetic response is almost negligible due to the fading field inside the sphere. On the other hand, the scattering of a Si NP includes electric and magnetic type resonance illustrated in Fig. 4(c), as previously shown in Fig. 3. Comparing the absorption cross-sections spectra in Fig. 4(b and d) for Ag Np and Si Np respectively, it is evident that the Si Np has less dissipative losses in comparison to its counterpart Ag NP.

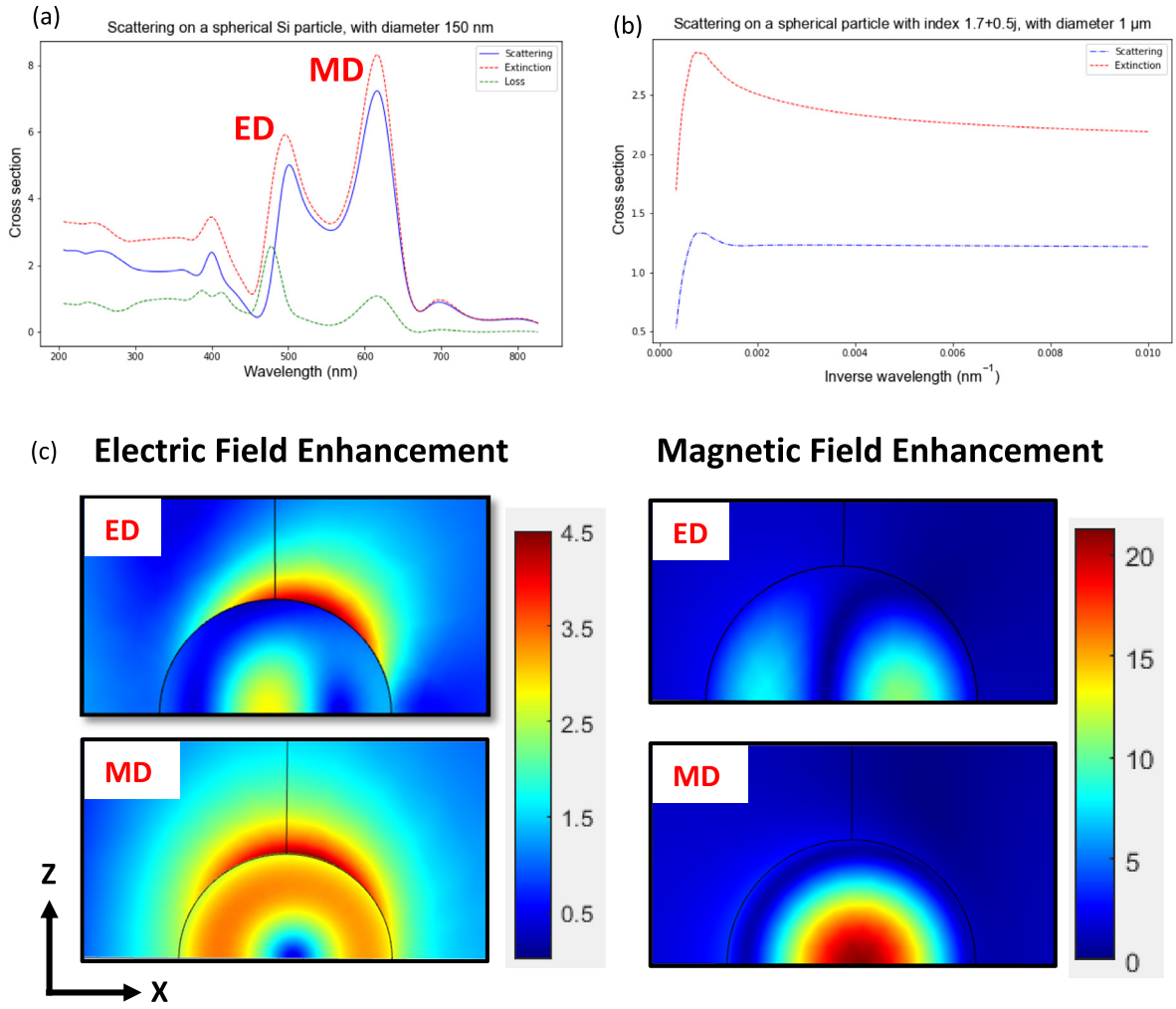

Fig. 3. Optical properties of spherical silicon particle. (a) Scattering, extinction and absorption cross-section for a Si NP of radius 75 nm using the dielectric properties of Si from (Aspnes and Studna, 1983). (b) Scattering from a theoretical dielectric sphere of diameter 1 μm. (c) Electric and magnetic field enhancement maps for electric dipole resonance (ED: upper figures) and magnetic dipole resonance (MD: lower figures).

Thus, strong magnetic Mie resonance modes are one of the main features of dielectric spheres. To empower such magnetic response in plasmonic structures, the metallic particle's geometry should be altered (Alu and Engheta, 2009; Monticone and Alù, 2014; Alù et al., 2006; Pendry et al., 1999) but then they will experience high ohmic losses and need a complicated fabrication procedure. Some of these geometries are split-ring resonators (Pendry et al., 1999) that enhances the magnetic field in the center.

Mie theory also proved that the maximized scattering efficiency for specific multipolar excitation of a subwavelength particle depends only on the resonance frequency and not the kind of the material (Schuller and Brongersma, 2009). Thus many plasmonic effects produced by metallic NPs can be realized with high-index dielectric nanoparticles taking advantage of the low dissipative losses of dielectric material compared to metallic ones.

Owing to the evolution of nanotechnology and nanophotonics, different geometries, other than spheres of dielectric nanoparticles, were fabricated based on the Mie resonance, such as spheroids (Fu et al., 2013; Luk'yanchuk et al., 2015), rings (van de Haar et al., 2016), cylinders (Evlyukhin et al., 2011), and other geometries (Zhang et al., 2013). This paves the way to different applications using this old theory such as third harmonic generation signals enhancement (Shcherbakov et al., 2014), the Raman signals (Dmitriev et al., 2016), spectroscopy (Albella et al., 2013), optical bio-sensing (Yavas et al., 2017), and light trapping in solar cells (Priolo et al., 2014; Wang et al., 2015). Optimizing the parameters of the designed structure will alter the position of the electric and magnetic dipole resonance which in turn will result in controlled emission directivity (Evlyukhin et al., 2011; Fu et al., 2013; Luk'yanchuk et al., 2015; Sinev, 2020; Staude et al., 2013 due to the overlap of both resonant type modes at the same wavelength. This phenomenon is discussed more in Section 4.3.

4. Enhancing light-matter interaction by dielectric materials

When a resonant cavity is in close proximity to a photoluminescent molecule, its properties are changed and, if the cavity is properly designed, a great enhancement in the PL signal can be achieved. For sensing applications, we are interested in enhancing the excitation rate, increasing the number of absorbed photons, enhance the radiative part of the decay rate, increasing the number of emitted photons (per absorbed photon), and also the capability of the adopted experimental setup to collect the emitted light, using controlled directivity. How these three phenomena (excitation-emission-collection) can be controlled with the introduction of a resonant dielectric cavity will be discussed in this section.

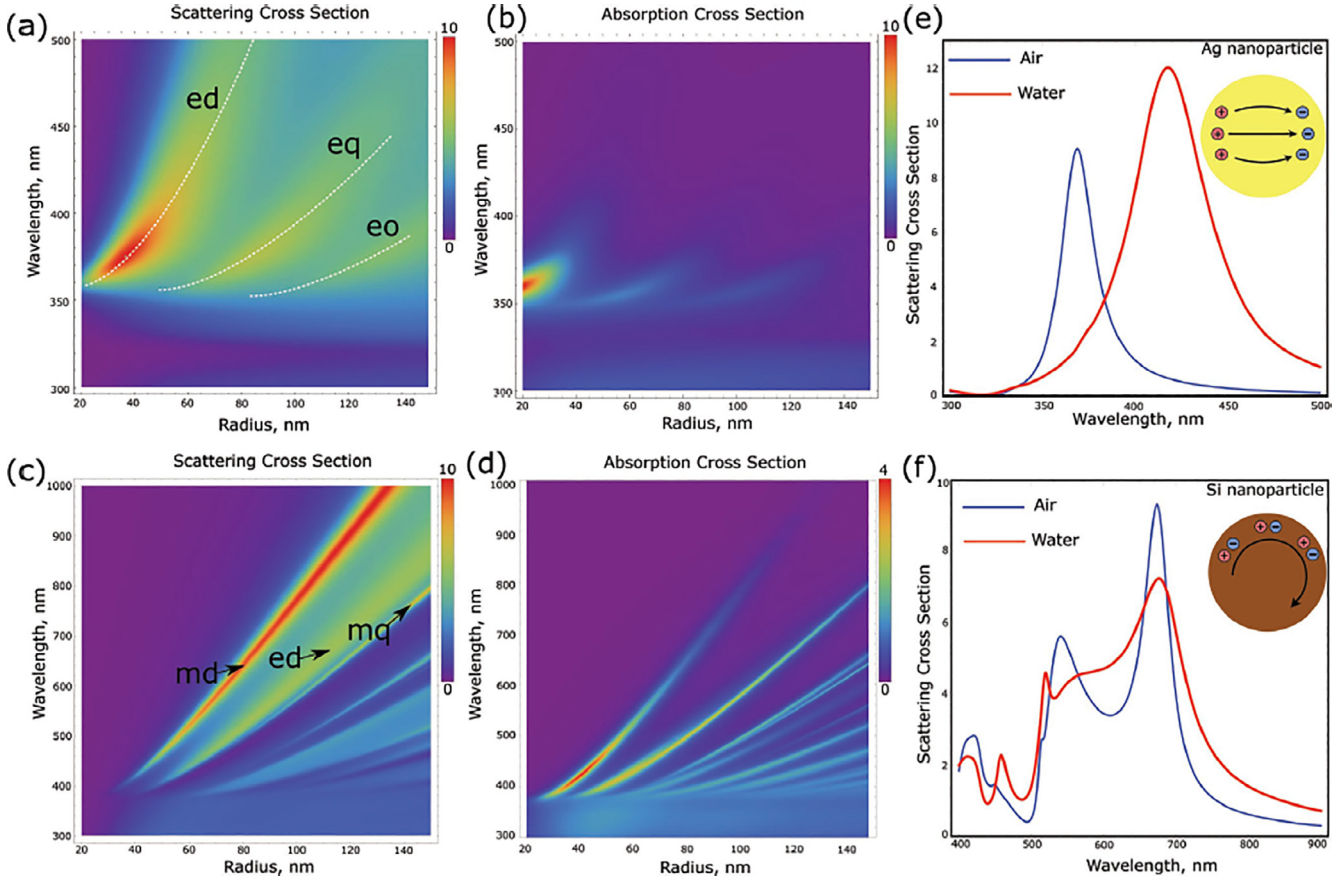

Fig. 4. Scattering and absorption cross-sections of metallic (Ag) and dielectric (Si) NPs. Variation of the normalized total scattering cross-section (Q_{sct}) of (a) the Ag NP and (c) the Si NP according to the radius and wavelength. Variation of the normalized absorption cross-section (Q_{abs}) of (b) the Ag NP and d) the Si NP, according to the radius and wavelength. Normalized scattering spectra of (e) the Ag NP of radius 30 nm and (f) the Si NP (of radius 85 nm) position in the air ($\varepsilon_h = 1$, blue curves) and water ($\varepsilon_h = 1.77$, red curves). Insets: schematic diagrams representing the fundamental modes of the metallic NP (plasmon dipole moment) and the dielectric NP (magnetic dipole Mie moment). Reproduced with permission (Krasnok et al., 2018). Copyright © 2018, John Wiley and Sons. (For interpretation of the references to color in this figure legend, the reader is referred to the web version of this article.)

4.1. Excitation rate enhancement

The absorption cross-section of an emitter (atoms, molecules, quantum dots, or the narrowband excitonic semiconductor states), linked to the excitation rate (γ_{exc}), is enhanced in the presence of a nanoscale resonator. Due to the ability of the nanoscale resonator to enhance and localize the electric field at sub-wavelength scales, the excitation/absorption cross-section of an emitter, considered as an electric dipole, can be defined as (Krasnok et al., 2018):

$$\sigma_{exc} = \sigma_0 \frac{|P.E|^2}{|P.E_0|^2} \tag{5}$$

where, σ_0 is the absorption cross-section of the molecule in the vacuum, P is the orientation of dipole, E and E_0 are respectively the electric field strength in the presence and absence of the resonator. Thus, the electric near field enhancement and localization achieved in the proximity of a nanostructure resonator will increase the excitation rate of an emitter placed near the resonator. Hence, we can define the excitation rate enhancement as

$$\gamma_{exc} = \frac{\sigma_{exc}}{\sigma_0} = \frac{|P \,.\, E|^2}{|P \,.\, E_0|^2} \tag{6}$$

that depends in general on the dipole orientation and location and the incident field intensity and polarization. To maximize this enhancement, the overlap of the maximum absorption wavelength of the emitter with the cavity resonant wavelength, where maximum field enhancement occurs, is required.

4.2. Emission enhancement

The presence of an emitter in the vicinity of the nanocavity will also alter the decay channels of an emitter when the emission wavelengths overlap with the resonant wavelengths. To understand the emission process, we need to fully understand the coupling between the emitter and the cavity. This can be understood by the simplest case of a two-level excited system in free space without a cavity, this is the so-called spontaneous emission, characterized by the decay rate given by the first-order perturbation theory by the Fermi Golden rule (Lukas Novotny, 2007)

$$\gamma^0_{mol} = \frac{2}{3}\frac{2\pi}{\hbar}(g_0\hbar)^2\left(\frac{\rho_0(\omega)}{\hbar}\right) \tag{7}$$

The coupling g_0 is given by $\sqrt{\frac{\omega d^2}{2\varepsilon_0 V\hbar}}$ for a dipole moment d and a quantization volume V, $\hbar$ is the reduced Planck constant. The density of state ρ_0 in free space is given by $\rho_0 \sim \int d\omega \frac{n\omega^2 V}{c^3}\delta(\omega - \omega_o)$, the decay rate of the molecule is then written as (the 2/3 factor comes from the vector nature of the dipole and the field)

$$\gamma^0_{mol} = \frac{1}{3\pi}\frac{nd^2\omega^3}{\hbar\varepsilon_0 c^3} \tag{8}$$

One can take advantage of changing the Dirac delta function in the density of state in free space by a Lorentzian distribution for a cavity

$$V\delta(\omega - \omega_o) \to \frac{2}{\pi}\frac{\gamma_c}{4(\omega - \omega_o)^2 + \gamma_c^2} \tag{9}$$

without the volume dependence, while the volume in the coupling constant is replaced by the field effective volume V_{eff}. The effective volume is usually defined as the integrated electric field squared divided by the maximum value of the squared electric field. Hence, near resonance $\omega \approx \omega_0$, the decay rate becomes, again by first order in perturbation theory assuming "small" coupling (Andreani et al., 1999);

$$\gamma_{mol} = \frac{2d^2\omega}{\hbar\varepsilon_0\varepsilon_r V_{eff}\gamma_c} \tag{10}$$

This phenomenon of modification of the spontaneous emission rate of molecules interacting with a resonant structure is known as the Purcell effect (Sauvan et al., 2013; Krasnok et al., 2015, 2016; de Torres et al., 2016). The ratio between the modified and free-space emission rate of a molecule is named Purcell factor (F_p) and can be computed as follows (Marquier et al., 2017):

$$F_p = \frac{\gamma_{mol}}{\gamma_{mol}^0} = \frac{3}{4\pi^2}\left(\frac{\lambda}{n}\right)^3 \frac{Q}{V_{eff}} \tag{11}$$

where λ is the transition wavelength and $Q = \omega/\gamma_c$ is the cavity quality factor. However, reducing the field volume may lead to strong coupling and hence need to go beyond first-order perturbation theory. A key idea comes from the analogy of the first-order perturbation result to that of a classical oscillator with strength. This analogy can be extended further to solve a strongly coupled cavity-emitter system by solving a simple coupled oscillator model (Reithmaier et al., 2004).

The classical approach was extensively verified for several configurations: quantum dots in nanoplasmonic resonators (Wu et al., 2010) coupling between nanocavity localized surface plasmon (LSP) and surface plasmon polaritons (SPP) (Chu et al., 2011). Some subtleties are found for the three-dimensional quantum box with nanopillar where the quantum open system master equation is needed.

Based on the coupling strength g, coupling a molecule to a dielectric or plasmonic nanocavity results basically in one of the two regimes of a spontaneous emission known as weak coupling and strong coupling regimes. Specifically, a strong coupling regime occurs if the value of coupling strength is greater than the total decay rate $g \geq \gamma$, where the total decay rate is $\gamma = \gamma_C + \gamma_{mol}$, in contrast, a system would be in a weak coupling case when the value of coupling strength is less than the total decay rate $g \leq \gamma$.

In a strong-coupling regime, photons will be diffused to the cavity mode faster than they escape. This implies that the cavity can re-excite the emitter, and energy will oscillate coherently back and forth, in a way known as vacuum Rabi oscillation (Khitrova et al., 2006; Savasta et al., 2010; Törmä and Barnes, 2015). This results in a more complex behavior of the spontaneous emission, which becomes non-exponential. In the strong coupling regime, the scattering cross-section will be that of a hybrid system emitter-cavity. Hence the definition of an enhancement with respect to the vacuum cross-section is a subtle issue.

Working now in the weak coupling regime, in general, the Purcell effect induces the enhancement of emission and dissipation rates. Due to the interest in the radiative part of spontaneous emission, we define the quantum yield of a molecular emitter as $\eta = \frac{\gamma_{mol}^{rad}}{\gamma_{mol}^{rad}+\gamma_{mol}^{loss}}$. Hence, the resulting enhancement of quantum yield of an emitter in the presence of the nanocavity can be expressed as:

$$\frac{\eta}{\eta_0} = \frac{\gamma_{mol}^{rad}/\gamma_{mol}^{0,rad}}{\eta_0((\gamma_{mol}^{rad}+\gamma_{mol}^{loss})/\gamma_{mol}^{0,rad}) + (1-\eta_0)} \tag{12}$$

where γ_{mol}^{rad} and γ_{mol}^{loss} are, respectively, the radiative and non-radiative decay rate of the molecule coupled to the nanocavity, and $\gamma_{mol}^{0,rad}$ is the radiative decay rate in the absence of the nanocavity.

4.3. Controlling the directivity

Any emitter characterized as dipolar or multipolar element will scatter light symmetrically in the plane transverse to the multipole axis. When the molecule is coupled to a resonant cavity, the symmetry is broken and a controlled directivity can be achieved. This will enhance the number of collected photons due to the enforcement of asymmetry scattering directed in a specific direction. The collection efficiency, which depends on the adopted experimental setup, is defined as the power emitted by the molecule that can be collected within a presumed range of polar angles normalized to the total power emitted to the far-field (Bauch and Dostalek, 2013).

Previous studies have shown that the separation between the emitter and the scatterer, and its polarizability play a crucial role in defining where a resonant structure acts as a collector or reflector (Rolly et al., 2011; Bonod et al., 2010). These behaviors are evident in Yagi-Uda antenna configuration achieved previously with plasmonic systems (Li et al., 2007; Taminiau et al., 2008), and then using all-dielectric based elements (Krasnok et al., 2011). Increasing the number of collector elements resulted in an enhanced directivity as was illustrated in (Krasnok et al., 2012).

Designing optical resonators play a key role in controlling the directivity of an emitter coupled to the resonator. Optimizing radiation emission patterns were successfully designed with plasmonic systems (Laux et al., 2017; Bauch and Dostalek, 2013; Aouani et al., 2011; Rodriguez et al., 2012; Zakharko et al., 2016). However, as previously mentioned, the limitations of plasmonic lead to the development of all-dielectric based structures, which attracted great interest recently since it can achieve the desired directionality with a more compact design, by exploiting the overlapping of the electric and magnetic dipole modes in resonant dielectric structures.

The use of dielectrics to collect light dates back to 1977 when a first study was performed using a dielectric substrate to collect light emission by electric dipole situated above the substrate (Lukosz and Kunz, 1977a, 1977b). Then microspheres composed of dielectric material were implemented a few years later to tailor the fluorescent signal of molecules through enhancing the excitation and improving the collection of the signals (Gérard et al., 2009; Aouani et al., 2009; Ghenuche et al., 2014; Yan et al., 2014). Furthermore, single silicon Np was used as a Huygens element in the optical range (Krasnok et al., 2011) demonstrating the so-called Kerker effect.

Kerker theory, established in 1983, described the condition of an ideal magnetic spherical particle. This theory stated that when illuminated from the far-field, the magnetic particle will scatter light in the forward direction with zero backward scattering when $\varepsilon = \mu$ (Kerker et al., 1983). This phenomenon was then extended in 2011 (Gómez-Medina, 2011; Nieto-Vesperinas et al., 2011) to explain the directionality from all-dielectric particles featuring both magnetic and electric dipole modes. Partially overlapping the electric and magnetic dipole modes in the spectrum results in observing the Kerker conditions and obtaining directional scattering in the forward or backward direction depending on the frequency. The first Kerker condition represents the domination of forward scattering at some wavelengths, while the domination of backward scattering at other wavelengths is known as the second Kerker condition (Rolly et al., 2012). Typically, a plane wave is used to excite a scatterer from the far-field region and establish the common Kerker condition, later this concept expanded to the near field where an electric dipole emitter excites a single high refractive index dielectric particle. Kerker effect is also feasible for more complex dielectric materials nanostructures and other high-order Mie resonant modes (Liu and Kivshar, 2017; Liu et al., 2015). The coupling between electric and magnetic dipole modes inducing a Kerker-type unidirectional scattering is demonstrated in many well-designed nanostructures composed of dielectric materials such as core–shell nanoparticles, cubic nanoantennas, dimer structures (Luk'yanchuk et al., 2015; Shibanuma et al., 2016; Tribelsky et al., 2016; Liu et al., 2012, 2014; Alaee et al., 2015; Dong et al., 2017; Sikdar et al., 2015; Li et al., 2015; Tian et al., 2016; Yao and Liu, 2016; Wiecha et al., 2017; Zhang et al., 2015; Wang et al., 2017). All-dielectric materials were also used to accomplish the directional con-

trol and enhancement of PL based on the Kerker effect in the near field excitation (Rolly et al., 2012, 2013).

The spectral overlapping between different multipolar modes can be achieved by engineering simple all-dielectric resonators and by controlling their size and shape, while more complex shapes are required in plasmonics to induce a magnetic and electric dipole in a resonator (Hancu et al., 2014; Proust et al., 2016; Coenen et al., 2014) or coupling different metallic nanowires (Dubois et al., 2018). Optimized tuning of the directivity is made possible by involving higher multipolar modes in the emission pattern.

To summarize what has been previously discussed, the enhancement in photoluminescence signal (fl) of emitters coupled to resonators is given as:

$$fl = \gamma_{exc} * \frac{\eta}{\eta_0} * \frac{\kappa_{coll}}{\kappa_{coll}^0} \tag{13}$$

where κ_{coll} and κ_{coll}^0 are the collection efficiency of the setup with and without the resonant structure, respectively. Collection efficiency is computed as shown in Eq. (14) considering the power emitted ($Pr(\theta, \varphi)$) in the accepted range of angles normalized to the total power emitted to the far-field (Bauch and Dostalek, 2013). The range of polar angles depends on the adopted experimental setup with a specific numerical aperture.

$$\kappa_{coll} = \frac{\int_0^{2\pi}\int_0^{\theta\_max} Pr(\theta,\varphi)\sin(\theta)d\theta d\varphi}{\int_0^{2\pi}\int_0^{\pi} Pr(\theta,\varphi)\sin(\theta)d\theta d\varphi} \tag{14}$$

Concluding this section, Eq. (13) shows that nanoantennas will play a crucial role in photoluminescence enhancement by (i) improving the excitation rate due to localized field enhancement (ii) enhanced emission decay rates, and reduce the non-radiative decay rates that will modify the quantum yield, and finally (iii) optimize emission directivity to enhance the collection efficiency of the optical setup.

5. Photoluminescence enhancement with resonant dielectric nanostructures

Plasmonics NPs have been broadly used in enhanced photoluminescence spectroscopy (Langguth et al., 2017; Luo et al., 2017), however, it suffers from high ohmic losses due to the absorption of metal. All-dielectric antennas featuring electromagnetic Mie resonances with weak losses have proven to be an alternative platform of plasmonics for PL enhancement. Featuring both electric and magnetic dipole Mie resonances, all-dielectric antennas allow an improved signal collection through directivity control (Krasnok et al., 2015), enhancing the excitation rates of emitters and tailoring their spontaneous emission rates avoiding any parasitic heating. Albella et al. (Albella et al., 2013) compared the behavior of silicon and gold dimers by computing the quantum yield and the radiative decay rates of a single electric dipole emitter placed in the gap of the dimer in both longitudinal and transversal orientations. This study proved that quantum yield enhancement achieved with Si antennas exceeded that of Au, thus demonstrating that dielectric antennas can yield a higher ratio between radiative and total decay rates due to their smaller intrinsic losses. Moreover, it has been shown in (Caldarola et al., 2015; Albella et al., 2014) that this enhancement is established with a negligible temperature increase in the hotspots of low loss dielectric dimer and its surroundings, overcoming the plasmonic limitations as illustrated in Fig. 5. Then in 2015, Staude et al. (Staude et al., 2015) demonstrated experimentally that coupling emitting quantum dots with resonant subwavelength silicon nanodisks will enhance its near infra-red PL spectrum. Maximum emission in a single direction was also achieved for the case of spectral overlap of the electric and magnetic dipolar resonances. This spectral overlap between the electric and magnetic resonance is controlled by optimizing the nanodisk dimensions. Knowing that dielectric NPs are characterized by their low absorption and absence of quenching, Sugimoto et al., in 2017 showed that PL signal enhancement up to 200 times of Rhodamine B dye molecules is achieved with one subwavelength silicon nanosphere and without any dielectric spacer between the nanosphere and the molecules (Sugimoto and Fujii, 2017). It was also proven in 2018 (Iwanaga, 2018), that all-dielectric metasurfaces are a potential platform for fluorescence enhancement, indeed, an array of silicon nanocylinders was designed to have its resonant wavelength as the working wavelength of the molecules. The experimental results show a 1000-fold enhancement of fluorescence intensity for a reference of a non-resonant flat Si wafer.

More complicated structures have been theoretically (Albella et al., 2013; Rolly et al., 2012) and experimentally (Caldarola et al., 2015; Cambiasso et al., 2017; Regmi et al., 2016) studied such as nanowires, dimers, trimers, and oligomers (Filonov et al., 2014; Bakker et al., 2015; Miri and Sadrara, 2017; Chong et al., 2014; Miroshnichenko and Kivshar, 2012; Habteyes et al., 2014). For instance, in (Caldarola et al., 2015), silicon disk dimers with a 20 nm gap were fabricated on a substrate exhibiting a near field enhancement in the gap, a homogenous thin-layer of dye molecules covers the silicon disk dimers allowing a controlled and uniform distribution of molecules on the nanoantennas, fluorescence enhancement in the vicinity of these structures is produced. The same approach was adopted in (Cambiasso et al., 2017) where coupling between dye molecules and dielectric materials was established using Gallium phosphide (GaP) as the nanoantenna material instead of silicon proving GaP nanoantennas as a promising material for second harmonic generation and fluorescence enhancement. The higher reported surface fluorescence enhancement achieved by GaP nanoantennas when compared to silicon in Fig. 6 is justified by the larger electric field intensity in the gap of the GaP nanoantennas and almost absence of losses in the visible range for GaP material, which triggers higher or improved emission enhancement.

Another approach is realized using freely diffusing dye molecules. This technique estimates the effect of the gap size on the fluorescence enhancement factor of a single-molecule. Dimer of silicon nanodisks with a 20 nm gap was implemented in (Regmi et al., 2016), featuring a broad dipolar resonance in the visible range with maximized near-field intensity in the gap in Fig. 7(b), which enhanced the fluorescence brightness by 270-fold outperforming gold structures with a similar gap as illustrated in Fig. 7(d). In this experimental approach, fluorescent molecules are spread out around the excited resonant nanostructure and fluorescence time traces are recorded. The clear bursts shown in Fig. 7(c) correspond to the single-molecule enhancement which occurs when the molecule diffuses into the gap where the enhanced electric field is localized, emitting many photons in a short time. The fluorescence enhancement factor for silicon and gold dimer are compared and results prove that dielectric-based structures can be an alternative platform to plasmonics avoiding any parasitic heating and quenching.

In 2016, another approach based on scanning probe microscopy was used, the near-field interaction at the nanoscale between fluorescence nanosphere and silicon nanoantennas with diameters varying between 170 nm and 250 nm was analyzed quantitatively (Bouchet et al., 2016). Furthermore, Vaskin et al. in 2018 experimentally demonstrated spectral and directional control of spontaneous emission from a coupled system of dielectric resonators with Fluorescence glass (Vaskin et al., 2018). The emission from the coupled system is enhanced when the antenna resonance overlaps with the intrinsic emission wavelength of the glass as shown in Fig. 7(e-f). Moreover, the authors also proved the ability of directional control of emission by matching the lattice period to the wavelength of the magnetic dipolar Mie-type resonance of nanocylinders which is a different mechanism from previous experimental demonstrations of directional emission enhancement (Vaskin et al., 2018). Then, Bohn et al., introduced the Liquid crystal (LC) cell to tune the resonance properties of

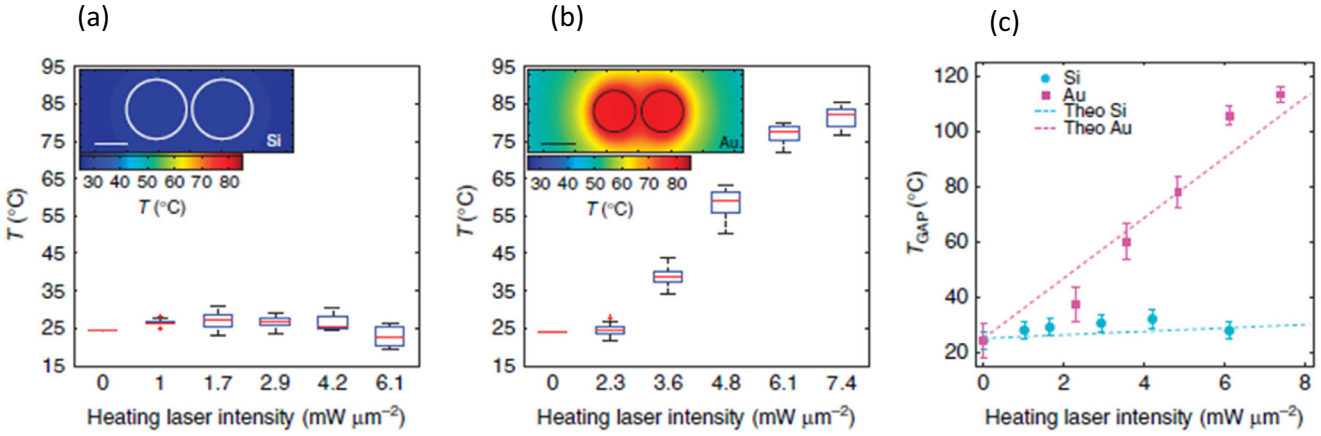

Fig. 5. Comparison of the temperature increase between Si and Au nanoantennas. (a–c) Temperature measurement in nanoantennas. Box plot for the average temperature T, measured for (a) silicon and (b) gold nanoantennas excited at resonance. The inset in each figure shows the calculated temperature map around the disks for the laser intensity of 5mWμm$^{(-2)}$ in both cases; Scale bar, 100 nm. (c) Extracted temperature in the gap for selected silicon (cyan) and gold (magenta) nanoantennas as a function of the heating laser intensity at 860 nm. The dashed lines show the numerical calculations for the temperature at the gap, presenting good agreement with the experimental data. The error bars show the standard deviation of the temperature measurements, obtained from error propagation from the fluorescence measurements. (a–c) Reproduced with permission (Caldarola et al., 2015). Copyright © 2015, Nature Publishing group. (For interpretation of the references to color in this figure legend, the reader is referred to the web version of this article.)

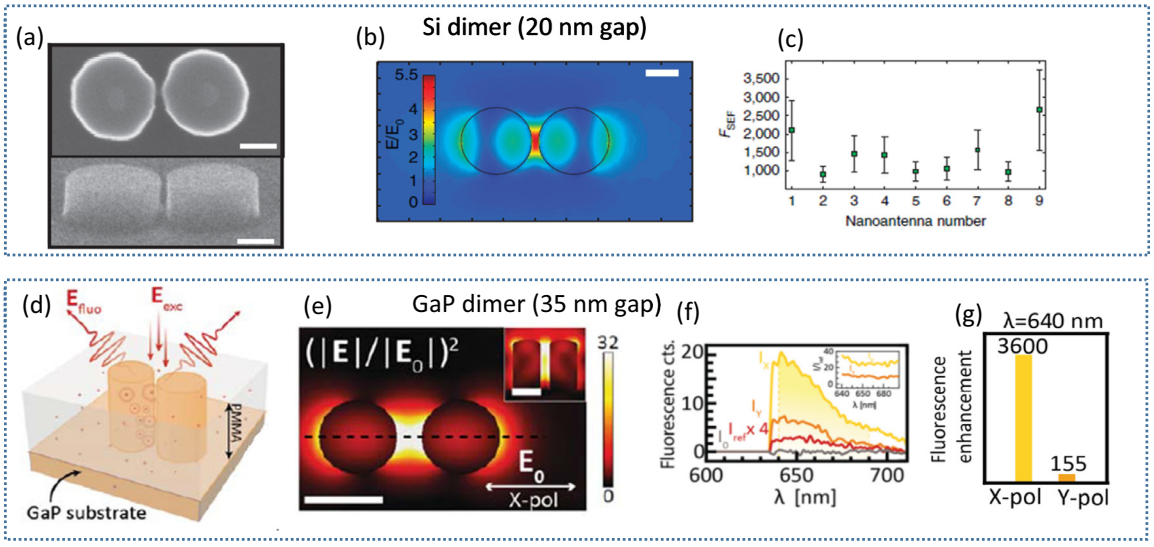

Fig. 6. All-dielectric nanoantenna for many molecules fluorescence enhancement. (a) SEM top-view (upper) and lateral-view (lower) images of a single nanoantenna of the array of nanostructures fabricated with Si on a silicon-on-insulator. Each nanoantenna consists of two identical disks with a 20-nm gap. Scale bar, 100 nm. (b) Near-field distribution map for the silicon structure excited at resonance, showing good confinement of the electric field in the gap. Scale bar, 100 nm. (c) Surface-enhanced fluorescence enhancement factor (FSEF) obtained from the maximum values over each antenna. (d) Experimental scheme of 35 nm gap GaP dimer covered by a polymer matrix with dyes embedded. (e) Normalized electric field intensity distribution for x-polarized excitation. (f) Fluorescence enhancement spectra using GaP dimers comparing the enhanced and initial fluorescence intensity, the sub-index X and Y indicate the polarization of the exciting laser. (g) Fluorescence enhancement factors of GaP dimer with 35 nm gap. (a–c) Reproduced with permission (Caldarola et al., 2015). Copyright © 2015, Nature Publishing Group. (d-g) Reproduced with permission (Cambiasso et al., 2017). Copyright © 2017, American Chemical Society.

the dielectric resonators. The transition of LC from nematic to the isotropic state via control of the cell temperature induces modification of metasurface resonance which results in an enhancement of spontaneous emission from the Fluorescent substrate owing to the Purcell effect (Bohn et al., 2018).

Taking advantage of the resonant modes found inside all-dielectric structures and their negligible losses, a novel strategy of coupling between emitters and dielectric resonators has been introduced based on integrating emitters inside the resonators. Recently in (Rutckaia et al., 2017), an experimental study of quantum dots coupled to silicon nanodisks illustrated in Fig. 8(a–c) demonstrated the enhancement of the photoluminescent signal from embedded quantum dots due to a well placement of the emitter with the Mie modes. Also in 2017, over three orders of PL enhancement of germanium quantum dots embedded in all-dielectric metasurfaces is experimentally observed accompanied with high-quality factor Fano resonance (Yuan et al., 2017). Another experimental study in 2018 shown in Fig. 8(d–f) demonstrated photoluminescence enhancement and directional reshaping of quantum dot emission by embedding self-assembled near-infrared InAs quantum dots in GaAs resonant metasurfaces (Liu et al., 2018).

A further promising approach for designing active dielectric Mie resonance for photoluminescence enhancement is to consider halide

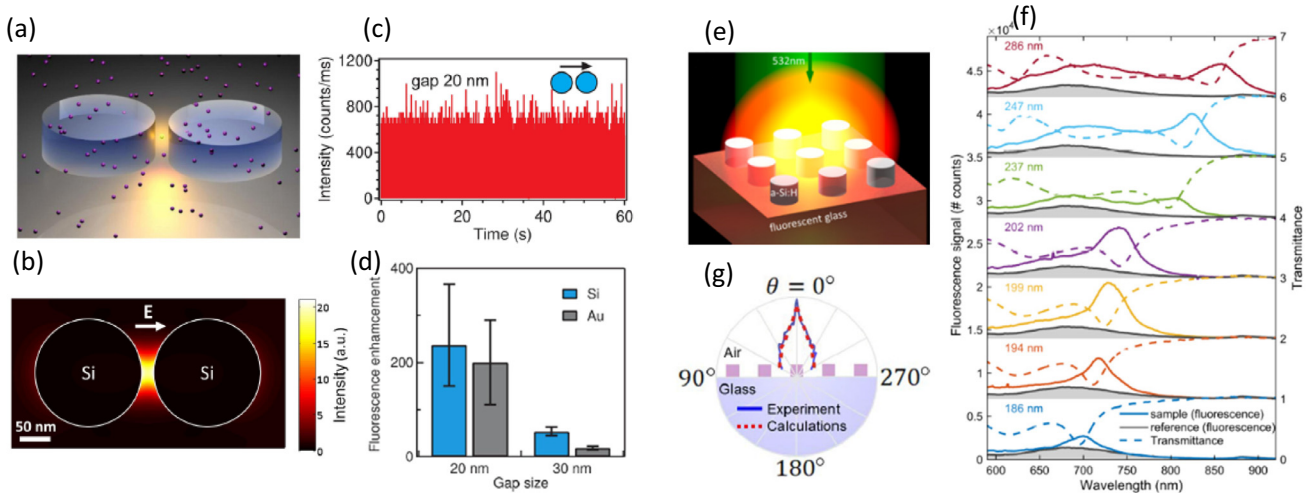

Fig. 7. Fluorescence enhancement approaches with resonant dielectric structures. (a) Schematic of silicon dimer antenna for fluorescence enhancement of single molecules freely diffusing in solution. (b) Electric field intensity enhancement map of silicon dimer. (c) Fluorescence bursts corresponding to a single molecule in the presence of 20 nm gap dimer. (d) Comparison of the fluorescence enhancement of Si and Au gap dimers as a function of gap length. (e) Schematic of Mie resonant nanocylinders composed of hydrogenated amorphous silicon (a-Si:H) placed on a fluorescent glass substrate illuminated at $\lambda = 532$ nm. (f) Experimentally measured emission spectra (solid lines) of varying diameters nanocylinder samples and its transmittance spectra (dotted lines) note that the reference shown in grey shading is the emission spectra of the bare glass substrate. (a–d) Reproduced with permission (Regmi et al., 2016). Copyright © 2016 American Chemical Society. (e–g) Reproduced with permission (Vaskin et al., 2018). Copyright © 2018 American Chemical Society.

perovskite. Halide perovskite is a type of semiconductor with high refractive index. It has been recently demonstrated in (Timpu et al., 2017) that second-harmonic generation enhancement is achieved using dielectric hybrid perovskite Mie resonances giving rise to many applications, such as those based on the lab-on-chip paradigm. Also enhanced PLof light-emitting nanoantenna as shown in Fig. 9(a-b) is realized by employing halide perovskite nanoparticles and coupling their excitons to the dipolar and multipolar Mie resonances (Tiguntseva et al., 2018). These novel materials with exceptional excitonic properties will lead to vast advancement in integrated light sources.

Recently, dielectric antennas based on Mie resonances have proven to enhance the photoluminescence signal of transition metal dichalcogenides (TMDC). They are cost-effective materials and atomically thin, making them an attractive material for several optoelectronic applications (Krasnok et al., 2018). In 2019, an analytical study of photoluminescence enhancement from different TMDC such as Wse_2, $MoSe_2$, WS_2, MoS_2 was performed. It was shown numerically that the PL signal of two-dimensional TMDC is enhanced by a factor of 100 when coupled to an optimized Si nanoantenna (Lepeshov et al., 2019). Also in 2019, GaP nanoantennas were designed and coupled to mono and bilayers of WSe_2 resulting in a PL enhancement of a factor of 10^4 compared to the same monolayer coupled to a planar GaP substrate as shown in Fig. 9(c), this enhancement results from a combination of enhanced excitation and emission rates and optimized directivity (Sortino et al., 2019).

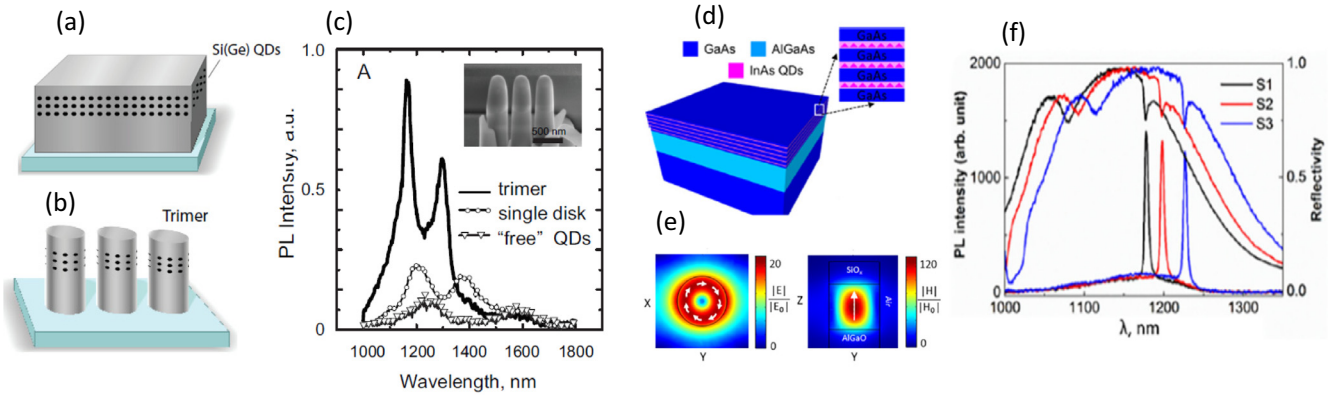

Fig. 8. Photoluminescence enhancement of embedded emitters in dielectric nanostructures. (a–b) Si(Ge) quantum dots embedded in silicon layers (left) and nanodisc Trimers. (c) PL spectra of a trimer (solid black line) shown on the inset having two sharp peaks at 1165 nm and 1302 nm with up to 10-fold intensity enhancement compared to the single disk emission (circles) and to the "free" Ge(Si) QDs (triangles). (d) Schematic of GaAs resonant metasurfaces incorporating several layers of self-assembled InAs quantum dots in its functional layer. (e) Numerical Electric and magnetic field mode profile in a cut plane through the nanocylinder of diameter 320 nm excited by a plane wave at $\lambda = 1200$ nm at an incident angle of $\theta = 20^\circ$ $\varphi = 0^\circ$. (f) Measured reflectance and corresponding photoluminescence spectra as a function of the metasurface geometry. (a–c) reproduced with permission (Rutckaia et al., 2017). Copyright © 2017 American Chemical Society. (d–f) reproduced with permission (Liu et al., 2018). Copyright © 2018 American Chemical Society.

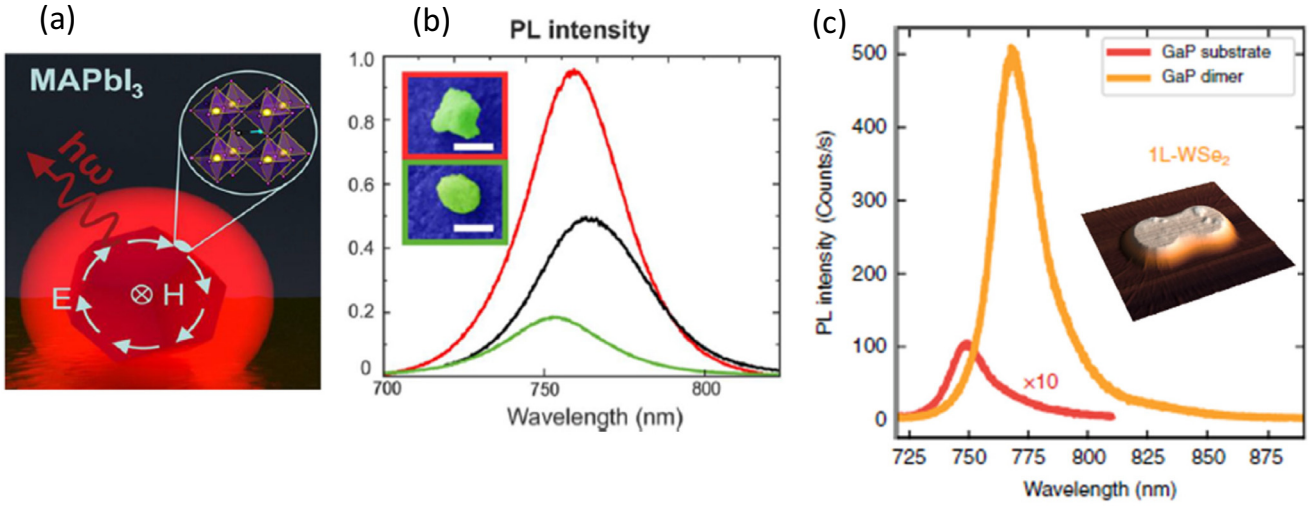

Fig. 9. Photoluminescence enhancement of various materials. (a) Schematic of tunable light-emitting halide perovskite nanoantenna acting both as the emitting material and as a Mie resonator and its (b) enhanced photoluminescence normalized to the volume for perovskite nanoparticles of different sizes shown in the inset with the SEM images matching the color of the frame with the color of the plot and compared with the PL spectrum of a 0.5 μm perovskite film. The scale bar is 400 nm. (c) PL spectra of 1 Layer-WSe_2 placed on GaP dimer (orange) and on a planar GaP substrate (red), its intensity is multiplied by 10 for comparison. Atomic force microscopic (AFM) image of a GaP nano-antenna covered with a monolayer WSe_2 is shown in the inset. (a-b) Reproduced with permission (Tiguntseva et al., 2018). Copyright © 2018 American Chemical Society. (c) Reproduced with permission (Sortino et al., 2019). Copyright © 2019 Nature publishing group. (For interpretation of the references to color in this figure legend, the reader is referred to the web version of this article.)

6. Conclusion & outlook

The summarized results prove that all-dielectric nanoantennas are a promising emerging field for photoluminescence enhancement in the visible and near-infrared range. In this review, we summarized the most recent developments within this emerging field. Starting from first principles, we show that dielectric material, featuring low optical losses, make it possible to realize resonant effects preventing high energy dissipation into heat and quenching of the emitted signal. This allows having a very low or even zero distance between the emitter and the resonator benefiting from the maximum enhanced field. Besides, dielectric based structures feature the coexistence of both electric and magnetic multipolar Mie resonant modes, and an engineered interference of these modes will result in controlled emission directivity. Dielectric resonant structures enhance the excitation and emission rates of emitters coupled to it by tailoring the decay rates of both electric and magnetic dipolar transitions. Not to forget the existence of strong fields inside the nanostructures that provide novel strategies for integrated quantum emitters inside dielectric structures. This has attracted the attention of researchers to use all-dielectric based structures in different applications including controllable quantum emitters, efficient multifunctional light modulators, flat-optics beam steering, and sensing applications.

Dielectric resonators reported in this review demonstrated their potential in enhancing photoluminescence of emitters, however, these results are still in lab-stage experiments. To efficiently apply such structures in optoelectronic devices and develop industrial prototypes, optimized designs and effective lower cost nanofabrication processes are needed. Interesting materials include different types of semiconductors, metal oxides, and insulators varying from high index to mid and low index materials. This variation of the refractive index and extinction coefficient allows the realization of various effects and their use in different applications.

Declaration of Competing Interest

The authors declare that they have no known competing financial interests or personal relationships that could have appeared to influence the work reported in this paper.

Acknowledgment

The work of Hiba Alhalaby and Haitham Zaraket was supported by the Project “Fibre Optic Sensors System for Irrigation Applications (FOSS4I),” funded by the U.K. Lebanon Tech HUB with CERN representative Martin Gastal as Project Manager. The FOSS4I Project is a collaboration among the following Institutes: The Lebanese University, Lebanese Agricultural Research Institute, National Instruments Lebanon, UK Lebanon TechHub, Saint Joseph University, INFN, University of Sannio, Optosmart, and CERN.

References

Alaee, R., Filter, R., Lehr, D., Lederer, F., Rockstuhl, C., 2015. A generalized Kerker condition for highly directive nanoantennas. Opt. Lett. 40, 2645. https://doi.org/10.1364/ol.40.002645.

Albella, P., Poyli, M.A., Schmidt, M.K., Maier, S.A., Moreno, F., Sáenz, J.José., Aizpurua, J., 2013. Low-Loss Electric and Magnetic Field-Enhanced Spectroscopy with Subwavelength Silicon Dimers. J. Phys. Chem. C. 117 (26), 13573–13584. https://doi.org/10.1021/jp4027018.

Albella, P., De La Osa, R.A., Moreno, F., Maier, S.A., 2014. Electric and magnetic field enhancement with ultralow heat radiation dielectric nanoantennas: considerations for surface-enhanced spectroscopies. ACS Photonics 1, 524–529. https://doi.org/10.1021/ph500060s.

Alu, A., Engheta, N., 2009. The quest for magnetic plasmons at optical frequencies. Opt. Express. 17, 5723. https://doi.org/10.1364/oe.17.005723.

Alù, A., Salandrino, A., Engheta, N., 2006. Negative effective permeability and left-handed materials at optical frequencies. Opt. Express. 14, 1557. https://doi.org/10.1364/oe.14.001557.

Andreani, L.C., Panzarini, G., Gérard, J.-M., 1999. Strong-coupling regime for quantum boxes in pillar microcavities: theory. Phys. Rev. B - Condens. Matter Mater. Phys. 60 (19), 13276–13279. https://doi.org/10.1103/PhysRevB.60.13276.

Aouani, H., Deiss, F., Wenger, J., Ferrand, P., Sojic, N., Rigneault, H., 2009. Optical-fiber-microsphere for remote fluorescence correlation spectroscopy. Opt. Express. 17 (21), 19085. https://doi.org/10.1364/OE.17.019085.

Aouani, H., Mahboub, O., Devaux, E., Rigneault, H., Ebbesen, T.W., Wenger, J., 2011. Plasmonic antennas for directional sorting of fluorescence emission. Nano Lett. 11 (6), 2400–2406. https://doi.org/10.1021/nl200772d.

Aspnes, D.E., Studna, A.A., 1983. Dielectric functions and optical parameters of Si, Ge, GaP, GaAs, GaSb, InP, InAs, and InSb from 1.5 to 6.0 eV. Phys. Rev. B 27, 985–1009. https://doi.org/10.1103/PhysRevB.27.985.

Bakker, R.M., Permyakov, D., Yu, Y.F., Markovich, D., Paniagua-Domínguez, R., Gonzaga, L., Samusev, A., Kivshar, Y., Luk'yanchuk, B., Kuznetsov, A.I., 2015. Magnetic and electric hotspots with silicon nanodimers. Nano Lett. 15 (3), 2137–2142. https://doi.org/10.1021/acs.nanolett.5b00128.

Barnes, M.D., Ng, K.C., Whitten, W.B., Ramsey, J.M., 1993. Detection of single rhodamine 6G molecules in levitated microdroplets. Anal. Chem. 65 (17), 2360–2365. https://doi.org/10.1021/ac00065a032.

Bauch, M., Dostalek, J., 2013. Collective localized surface plasmons for high performance fluorescence biosensing. Opt. Express. 21, 20470. https://doi.org/10.1364/oe.21.020470.

Bliokh, K.Y., Bliokh, Y.P., Freilikher, V., Savel'ev, S., Nori, F., 2008. Colloquium: Unusual resonators: Plasmonics, metamaterials, and random media, Rev. Mod. Phys. 80, 1201–1213. 10.1103/RevModPhys.80.1201.

Bohn, J., Bucher, T., Chong, K.E., Komar, A., Choi, D., Neshev, D.N., Kivshar, Y.S., Pertsch, T., Staude, I., Neshev, D.N., Kivshar, Y.S., Pertsch, T., 2018. Active tuning of spontaneous emission by Mie-resonant dielectric metasurfaces. Nano Lett. 18, 3461–3465. https://doi.org/10.1021/acs.nanolett.8b00475.

Bohren, C.F., 1983. Absorption and Scattering of Light by Small Particles. John Wiley Sons. 10.1088/0031-9112/35/3/025.

Bohren, C.F., Huffman, D.R., 1998. Absorption and Scattering of Light by Small Particles. Wiley. 10.1002/9783527618156.

Bonod, N., Devilez, A., Rolly, B., Bidault, S., Stout, B., 2010. Ultracompact and unidirectional metallic antennas. Phys. Rev. B – Condens. Matter Mater. Phys. 82,. https://doi.org/10.1103/PhysRevB.82.115429 115429.

Bouchet, D., Mivelle, M., Proust, J., Gallas, B., Ozerov, I., Maria, F., Gulinatti, A., Rech, I., De Wilde, Y., Bonod, N., Krachmalnicoff, V., Bidault, S., 2016. Enhancement and inhibition of spontaneous photon emission by resonant silicon nanoantennas. Phys. Rev. Appl. 6, 1–22.

Caldarola, M., Albella, P., Cortés, E., Rahmani, M., Roschuk, T., Grinblat, G., Oulton, R. F., Bragas, A.V., Maier, S.A., 2015. Non-plasmonic nanoantennas for surface enhanced spectroscopies with ultra-low heat conversion. Nat. Commun. 6 (1). https://doi.org/10.1038/ncomms8915.

Cambiasso, J., Grinblat, G., Li, Y., Rakovich, A., Cortés, E., Maier, S.A., 2017. Bridging the gap between dielectric nanophotonics and the visible regime with effectively lossless gallium phosphide antennas. Nano Lett. 17 (2), 1219–1225. https://doi.org/10.1021/acs.nanolett.6b05026.

Chong, K.E., Hopkins, B., Staude, I., Miroshnichenko, A.E., Dominguez, J., Decker, M., Neshev, D.N., Brener, I., Kivshar, Y.S., 2014. Observation of fano resonances in all-dielectric nanoparticle oligomers. Small. 10 (10), 1985–1990. https://doi.org/10.1002/smll.201303612.

Chu, Y., Wang, D., Zhu, W., Crozier, K.B., 2011. Double resonance surface enhanced Raman scattering substrates: an intuitive coupled oscillator model. Opt. Express. 19, 14919. https://doi.org/10.1364/oe.19.014919.

Coenen, T., Bernal Arango, F., Femius Koenderink, A., Polman, A., 2014. Directional emission from a single plasmonic scatterer. Nat. Commun. 5, 1–8. https://doi.org/10.1038/ncomms4250.

de Torres, J., Ferrand, P., Colas des Francs, G., Wenger, J., 2016. Coupling emitters and silver nanowires to achieve long-range plasmon-mediated fluorescence energy transfer. ACS Nano 10 (4), 3968–3976. https://doi.org/10.1021/acsnano.6b00287.

Dmitriev, P.A., Baranov, D.G., Milichko, V.A., Makarov, S.V., Mukhin, I.S., Samusev, A. K., Krasnok, A.E., Belov, P.A., Kivshar, Y.S., 2016. Resonant Raman scattering from silicon nanoparticles enhanced by magnetic response. Nanoscale. 8 (18), 9721–9726. https://doi.org/10.1039/C5NR07965A.

Dong, Z., Ho, J., Yu, Y.F., Fu, Y.H., Paniagua-Dominguez, R., Wang, S., Kuznetsov, A.I., Yang, J.K.W., 2017. Printing beyond sRGB color gamut by mimicking silicon nanostructures in free-space. Nano Lett. 17 (12), 7620–7628. https://doi.org/10.1021/acs.nanolett.7b0361310.1021/acs.nanolett.7b03613.s001.

Adam Dorfman, Nitin Kumar, Hahm, J., 2006. Highly Sensitive Biomolecular Fluorescence Detection Using Nanoscale ZnO Platforms. 10.1021/LA053270+.

Dubois, M., Leroi, L., Raolison, Z., Abdeddaim, R., Antonakakis, T., De Rosny, J., Vignaud, A., Sabouroux, P., Georget, E., Larrat, B., Tayeb, G., Bonod, N., Amadon, A., Mauconduit, F., Poupon, C., Le Bihan, D., Enoch, S., 2018. Kerker effect in ultrahigh-field magnetic resonance imaging. Phys. Rev. X. 8, 31083. https://doi.org/10.1103/PhysRevX.8.031083.

Eigen, M., Rigler, R., 1994. Sorting single molecules: application to diagnostics and evolutionary biotechnology. Proc. Natl. Acad. Sci. U. S. A. 91 (13), 5740–5747. https://doi.org/10.1073/pnas.91.13.5740.

Evlyukhin, A.B., Reinhardt, C., Seidel, A., Luk'yanchuk, B.S., Chichkov, B.N., 2010. Optical response features of Si-nanoparticle arrays. Phys. Rev. B - Condens. Matter Mater. Phys. 82 (4). https://doi.org/10.1103/PhysRevB.82.045404.

Evlyukhin, A.B., Reinhardt, C., Chichkov, B.N., 2011. Multipole light scattering by nonspherical nanoparticles in the discrete dipole approximation. Phys. Rev. B – Condens. Matter Mater. Phys. 84. https://doi.org/10.1103/PhysRevB.84.235429.

Evlyukhin, A.B., Novikov, S.M., Zywietz, U., Eriksen, R.L., Reinhardt, C., Bozhevolnyi, S. I., Chichkov, B.N., 2012. Demonstration of magnetic dipole resonances of dielectric nanospheres in the visible region. Nano Lett. 12 (7), 3749–3755. https://doi.org/10.1021/nl301594s.

Filonov, D.S., Slobozhanyuk, A.P., Krasnok, A.E., Belov, P.A., Nenasheva, E.A., Hopkins, B., Miroshnichenko, A.E., Kivshar, Y.S., 2014. Near-field mapping of Fano resonances in all-dielectric oligomers. Appl. Phys. Lett. 104, 21104. https://doi.org/10.1063/1.4858969.

Fu, Y.H., Kuznetsov, A.I., Miroshnichenko, A.E., Yu, Y.F., Luk'yanchuk, B., 2013. Directional visible light scattering by silicon nanoparticles. Nat. Commun. 4, 1–6. https://doi.org/10.1038/ncomms2538.

Ganesh, N., Zhang, W., Mathias, P.C., Chow, E., Soares, J.A.N.T., Malyarchuk, V., Smith, A.D., Cunningham, B.T., 2007. Enhanced fluorescence emission from quantum dots on a photonic crystal surface. Nat. Nanotechnol. 2 (8), 515–520. https://doi.org/10.1038/nnano.2007.216.

García-Etxarri, A., Gómez-Medina, R., Froufe-Pérez, L.S., López, C., Chantada, L., Scheffold, F., Aizpurua, J., Nieto-Vesperinas, M., Sáenz, J.J., 2011. Strong magnetic response of submicron Silicon particles in the infrared. Opt. Express. 19, 4815. https://doi.org/10.1364/oe.19.004815.

Geddes, C.D., Lakowicz, J.R., 2002. Metal-Enhanced Fluorescence concentrating the local field and subsequently increasing.

Gérard, D., Devilez, A., Aouani, H., Stout, B., Bonod, N., Wenger, J., Popov, E., Rigneault, H., 2009. Efficient excitation and collection of single-molecule fluorescence close to a dielectric microsphere. J. Opt. Soc. Am. B. 26, 1473. https://doi.org/10.1364/josab.26.001473.

Gerber, S., Reil, F., Hohenester, U., Schlagenhaufen, T., Krenn, J.R., Leitner, A., 2007. Tailoring light emission properties of fluorophores by coupling to resonance-tuned metallic nanostructures. Phys. Rev. B – Condens. Matter Mater. Phys. 75, 73404. https://doi.org/10.1103/PhysRevB.75.073404.

Ghenuche, P., De Torres, J., Ferrand, P., Wenger, J., 2014. Multi-focus parallel detection of fluorescent molecules at picomolar concentration with photonic nanojets arrays. Appl. Phys. Lett.. https://doi.org/10.1063/1.4896852. 131102.

Goldys, E.M., Drozdowicz-Tomsia, K., Xie, F., Shtoyko, T., Matveeva, E., Gryczynski, I., Gryczynski, Z., 2007. Fluorescence amplification by electrochemically deposited silver nanowires with fractal architecture. J. Am. Chem. Soc. 129 (40), 12117–12122. https://doi.org/10.1021/ja071981j.

Gómez-Medina, R., 2011. Electric and magnetic dipolar response of germanium nanospheres: interference effects, scattering anisotropy, and optical forces. J. Nanophotonics. 5, 53512. https://doi.org/10.1117/1.3603941.

Gu, C., Huang, J., Ni, N., Li, M., Liu, J., 2008. Detection of DNA hybridization based on SnO2 nanomaterial enhanced fluorescence. J. Phys. D. Appl. Phys. 41,. https://doi.org/10.1088/0022-3727/41/17/175103 175103.

Habteyes, T.G., Staude, I., Chong, K.E., Dominguez, J., Decker, M., Miroshnichenko, A., Kivshar, Y., Brener, I., 2014. Near-field mapping of optical modes on all-dielectric silicon nanodisks. ACS Photonics 1 (9), 794–798. https://doi.org/10.1021/ph500232u.

Hancu, I.M., Curto, A.G., Castro-López, M., Kuttge, M., van Hulst, N.F., 2014. Multipolar interference for directed light emission. Nano Lett. 14 (1), 166–171. https://doi.org/10.1021/nl403681g.

Hergert, W., 2012. Gustav mie: from electromagnetic scattering to an electromagnetic view of matter. Springer Ser. Opt. Sci. 169, 1–51. https://doi.org/10.1007/978-3-642-28738-1_1.

Smolyaninov, I.I., Hung, Y.J., Davis, C.C., 2007. Fluorescence enhancement by surface gratings, in: Opt. InfoBase Conf. Pap., Optical Society of America, 2007: pp. 10825–10830. 10.1364/oe.14.010825.

Iwanaga, M., 2018. All-dielectric metasurfaces with high-fluorescence-enhancing capability. Appl. Sci. 8, 1328. https://doi.org/10.3390/app8081328.

Jin, J.-M., 2015. The Finite Element Method in Electromagnetics. John Wiley & Sons.

Kerker, M., Wang, D.S., Giles, C.L., 1983. Electromagnetic scattering by magnetic spheres. J. Opt. Soc. Am. 73, 765–767. https://doi.org/10.1364/JOSA.73.000765.

Khitrova, G., Gibbs, H.M., Kira, M., Koch, S.W., Scherer, A., 2006. Vacuum Rabi splitting in semiconductors. Nat. Phys. 2 (2), 81–90. https://doi.org/10.1038/nphys227.

Koenderink, A.F., 2017. Single-photon nanoantennas. ACS Photonics 4 (4), 710–722. https://doi.org/10.1021/acsphotonics.7b00061.

Krasnok, A., Glybovski, S., Petrov, M., Makarov, S., Savelev, R., Belov, P., Simovski, C., Kivshar, Y., 2016. Demonstration of the enhanced Purcell factor in all-dielectric structures. Appl. Phys. Lett. 108,. https://doi.org/10.1063/1.4952740 211105.

Krasnok, A., Lepeshov, S., Alú, A., 2018. Nanophotonics with 2D transition metal dichalcogenides. arXiv. 26, 15972–15994. https://doi.org/10.1364/OE.26.015972.

Krasnok, A., Caldarola, M., Bonod, N., Alú, A., 2018. Spectroscopy and biosensing with optically resonant dielectric nanostructures. Adv. Opt. Mater. 6, 1–22. https://doi.org/10.1002/adom.201701094.

Krasnok, A.E., Miroshnichenko, A.E., Belov, P.A., Kivshar, Y.S., 2011. Huygens optical elements and Yagi-Uda nanoantennas based on dielectric nanoparticles. JETP Lett. 94 (8), 593–598. https://doi.org/10.1134/S0021364011200070.

Krasnok, A.E., Miroshnichenko, A.E., Belov, P.A., Kivshar, Y.S., 2012. All-dielectric optical nanoantennas. Opt. Express. 20, 20599. https://doi.org/10.1364/oe.20.020599.

Krasnok, A.E., Maloshtan, A., Chigrin, D.N., Kivshar, Y.S., Belov, P.A., 2015. Enhanced emission extraction and selective excitation of NV centers with all-dielectric nanoantennas. Laser Photon. Rev. 9 (4), 385–391. https://doi.org/10.1002/lpor.201400453.

Krasnok, A.E., Slobozhanyuk, A.P., Simovski, C.R., Tretyakov, S.A., Poddubny, A.N., Miroshnichenko, A.E., Kivshar, Y.S., Belov, P.A., 2015. An antenna model for the Purcell effect. Sci. Rep. 5, 1–16. https://doi.org/10.1038/srep12956.

Kuznetsov, A.I., Miroshnichenko, A.E., Fu, Y.H., Zhang, J., Lukyanchukl, B., 2012. Magnetic light. Sci. Rep. 2, 1–6. https://doi.org/10.1038/srep00492.

Lakowicz, J.R., 2006. Principles of Fluorescence Spectroscopy. Springer. 10.1007/978-0-387-46312-4.

Langguth, L., Szuba, A., Mann, S.A., Garnett, E.C., Koenderink, G.H., Koenderink, A.F., 2017. Nano-antenna enhanced two-focus fluorescence correlation spectroscopy/639/925/927/1021/639/624/1107/328 article. Sci. Rep. 7, 1–9. https://doi.org/10.1038/s41598-017-06325-6.

Laux, F., Bonod, N., Gérard, D., 2017. Single emitter fluorescence enhancement with surface lattice resonances. J. Phys. Chem. C. 121 (24), 13280–13289. https://doi.org/10.1021/acs.jpcc.7b04207.

Lepeshov, S., Krasnok, A., Alu, A., 2019. Enhanced excitation and emission from 2D transition metal dichalcogenides with all-dielectric nanoantennas. Nanotechnology. 30,. https://doi.org/10.1088/1361-6528/ab0daf 254004.

Li, W.-D., Ding, F., Hu, J., Chou, S.Y., 2011. Three-dimensional cavity nanoantenna coupled plasmonic nanodots for ultrahigh and uniform surface-enhanced Raman scattering over large area. Opt. Express. 19, 3925. https://doi.org/10.1364/oe.19.003925.

Li, J., Salandrino, A., Engheta, N., 2007. Shaping light beams in the nanometer scale: A Yagi-Uda nanoantenna in the optical domain. Phys. Rev. B – Condens. Matter Mater. Phys. 76,. https://doi.org/10.1103/PhysRevB.76.245403 245403.

Li, Y., Wan, M., Wu, W., Chen, Z., Zhan, P., Wang, Z., 2015. Broadband zero-backward and near-zero-forward scattering by metallo-dielectric core-shell nanoparticles. Sci. Rep. 5, 12491. https://doi.org/10.1038/srep12491.

Lichtman, J.W., Conchello, J.-A., 2005. Fluorescence microscopy. Nat. Methods 2 (12), 910–919. https://doi.org/10.1038/nmeth817.

Liu, W., Kivshar, Y.S., 2017. Generalized Kerker effects in nanophotonics and meta-optics. arXiv. 26, 274–284. https://doi.org/10.1364/OE.26.013085.

Liu, W., Miroshnichenko, A.E., Neshev, D.N., Kivshar, Y.S., 2012. Broadband unidirectional scattering by magneto-electric core-shell nanoparticles. ACS Nano 6 (6), 5489–5497. https://doi.org/10.1021/nn301398a.

Liu, S., Vaskin, A., Addamane, S., Leung, B., Tsai, M., Yang, Y., Vabishchevich, P.P., Keeler, G.A., Wang, G., He, X., Kim, Y., Hartmann, N.F., Htoon, H., Doorn, S.K., Zilk, M., Pertsch, T., Balakrishnan, G., Sinclair, M.B., Staude, I., Brener, I., 2018. Light-emitting metasurfaces: simultaneous control of spontaneous emission and far-field radiation. Nano Lett. 18, 6906–6914. https://doi.org/10.1021/acs.nanolett.8b02808.

Liu, W., Zhang, J., Lei, B., Ma, H., Xie, W., Hu, H., 2014. Ultra-directional forward scattering by individual core-shell nanoparticles. Opt. Express. 22, 16178. https://doi.org/10.1364/oe.22.016178.

Liu, W., Kuznetsov, A.I., Miroshnichenko, A.E., Fu, Y.H., Zhang, J.B., Lukyanchuk, B. S., 2015. Ultra-directional super-scattering of homogenous spherical particles with radial anisotropy. Opt. Express. 23, 14734. https://doi.org/10.1364/oe.23.014734.

Lu, G., Li, W., Zhang, T., Yue, S., Liu, J., Hou, L., Li, Z., Gong, Q., 2012. Plasmonic-enhanced molecular fluorescence within isolated bowtie nano-apertures. ACS Nano 6 (2), 1438–1448. https://doi.org/10.1021/nn2042412.

Luk'yanchuk, B.S., Voshchinnikov, N.V., Paniagua-Domínguez, R., Kuznetsov, A.I., 2015. Optimum forward light scattering by spherical and spheroidal dielectric nanoparticles with high refractive index. ACS Photonics 2 (7), 993–999. https://doi.org/10.1021/acsphotonics.5b00261.

Lukas Novotny, B.H., 2007. Principles of Nano-optics Second edition.

Lukosz, W., Kunz, R.E., 1977a. Light emission by magnetic and electric dipoles close to a plane dielectric interface II Radiation patterns of perpendicular oriented dipoles. J. Opt. Soc. Am. 67, 1615. https://doi.org/10.1364/josa.67.001615.

Lukosz, W., Kunz, R.E., 1977b. Light emission by magnetic and electric dipoles close to a plane interface I Total radiated power. J. Opt. Soc. Am. 67, 1607. https://doi.org/10.1364/josa.67.001607.

Luo, S., Li, Q., Yang, Y., Chen, X., Wang, W., Qu, Y., Qiu, M., 2017. Controlling fluorescence emission with split-ring-resonator-based plasmonic metasurfaces. Laser Photon. Rev. 11 (3), 1600299. https://doi.org/10.1002/lpor.201600299.

Malicka, J., Gryczynski, I., Fang, J., Kusba, J., Lakowicz, J.R., 2003. Increased resonance energy transfer between fluorophores bound to DNA in proximity to metallic silver particles. Anal. Biochem. 315 (2), 160–169. https://doi.org/10.1016/S0003-2697(02)00710-8.

Marquier, F., Sauvan, C., Greffet, J.-J., 2017. Revisiting quantum optics with surface plasmons and plasmonic resonators. ACS Photonics 4 (9), 2091–2101. https://doi.org/10.1021/acsphotonics.7b00475.

Mie, G., 1908. Beiträge zur Optik trüber Medien, speziell kolloidaler Metallösungen. Ann. Phys. 330 (3), 377–445. https://doi.org/10.1002/(ISSN)1521-388910.1002/andp.19083300302.

Miri, M., Sadrara, M., 2017. Dimers and trimers of hollow silicon nanoparticles: manipulating the magnetic hotspots. J. Phys. Chem. C. 121 (21), 11672–11679. https://doi.org/10.1021/acs.jpcc.7b02351.

Miroshnichenko, A.E., Kivshar, Y.S., 2012. Fano resonances in all-dielectric oligomers. Nano Lett. 12 (12), 6459–6463. https://doi.org/10.1021/nl303927q.

Molinari, G., 2015. Fluorescence Microscopy for Microbiology. Springer, Berlin, Heidelberg, pp. 49–69. 10.1007/8623_2015_108.

Monticone, F., Alù, A., 2014. The quest for optical magnetism: from split-ring resonators to plasmonic nanoparticles and nanoclusters. J. Mater. Chem. C. 2, 9059–9072. https://doi.org/10.1039/c4tc01406e.

Mukundan, H., Xie, H., Anderson, A.S., Grace, W.K., Shively, J.E., Swanson, B.I., 2009. Optimizing a waveguide-based sandwich immunoassay for tumor biomarkers: evaluating fluorescent labels and functional surfaces. Bioconjug. Chem. 20, 222–230. https://doi.org/10.1021/bc800283e.

Nieto-Vesperinas, M., Gomez-Medina, R., Saenz, J.J., 2011. Angle-suppressed scattering and optical forces on submicrometer dielectric particles. J. Opt. Soc. Am. A. 28, 54. https://doi.org/10.1364/josaa.28.000054.

Pendry, J.B., Holden, A.J., Robbins, D.J., Stewart, W.J., 1999. Magnetism from conductors and enhanced nonlinear phenomena. IEEE Trans. Microw. Theory Tech. 47, 2075–2084. https://doi.org/10.1109/22.798002.

Perkowitz, S., 2012. Optical Characterization of Semiconductors: Infrared, Raman, and Photoluminescence Spectroscopy. Elsevier.

Priolo, F., Gregorkiewicz, T., Galli, M., Krauss, T.F., 2014. Silicon nanostructures for photonics and photovoltaics. Nat. Nanotechnol. 9 (1), 19–32. https://doi.org/10.1038/nnano.2013.271.

Proust, J., Bonod, N., Grand, J., Gallas, B., 2016. Optical monitoring of the magnetoelectric coupling in individual plasmonic scatterers. ACS Photonics 3 (9), 1581–1588. https://doi.org/10.1021/acsphotonics.6b00041.

Regmi, R., Berthelot, J., Winkler, P.M., Mivelle, M., Proust, J., Bedu, F., Ozerov, I., Begou, T., Lumeau, J., Rigneault, H., García-Parajó, M.F., Bidault, S., Wenger, J., Bonod, N., 2016. All-dielectric silicon nanogap antennas to enhance the fluorescence of single molecules. Nano Lett. 16 (8), 5143–5151. https://doi.org/10.1021/acs.nanolett.6b02076.

Reithmaier, J.P., Sęk, G., Löffler, A., Hofmann, C., Kuhn, S., Reitzenstein, S., Keldysh, L. V., Kulakovskii, V.D., Reinecke, T.L., Forchel, A., 2004. Strong coupling in a single quantum dot-semiconductor microcavity system. Nature 432 (7014), 197–200. https://doi.org/10.1038/nature02969.

Resch-Genger, U., Grabolle, M., Cavaliere-Jaricot, S., Nitschke, R., Nann, T., 2008. Quantum dots versus organic dyes as fluorescent labels. Nat. Methods 5 (9), 763–775. https://doi.org/10.1038/nmeth.1248.

Rodriguez, S.R.K., Lozano, G., Verschuuren, M.A., Gomes, R., Lambert, K., De Geyter, B., Hassinen, A., Van Thourhout, D., Hens, Z., Gómez Rivas, J., 2012. Quantum rod emission coupled to plasmonic lattice resonances: a collective directional source of polarized light. Appl. Phys. Lett. 100,. https://doi.org/10.1063/1.3693397 111103.

Rolly, B., Stout, B., Bonod, N., 2012. Boosting the directivity of optical antennas with magnetic and electric dipolar resonant particles Abstract, 20 (2012) 1473–1478.

Rolly, B., Stout, B., Bidault, S., Bonod, N., 2011. Crucial role of the emitter–particle distance on the directivity of optical antennas. Opt. Lett. 36, 3368. https://doi.org/10.1364/ol.36.003368.

Rolly, B., Stout, B., Bonod, N., 2012. Boosting the directivity of optical antennas with magnetic and electric dipolar resonant particles. Opt. Express. 20, 20376. https://doi.org/10.1364/oe.20.020376.

Rolly, B., Bebey, B., Bidault, S., Stout, B., Bonod, N., 2012. Promoting magnetic dipolar transition in trivalent lanthanide ions with lossless Mie resonances. Phys. Rev. B – Condens. Matter Mater. Phys. 85,. https://doi.org/10.1103/PhysRevB.85.245432 245432.

Rolly, B., Geffrin, J.-M., Abdeddaim, R., Stout, B., Bonod, N., 2013. Controllable emission of a dipolar source coupled with a magneto-dielectric resonant subwavelength scatterer. Sci. Rep. 3 (1). https://doi.org/10.1038/srep03063.

Rutckaia, V., Heyroth, F., Novikov, A., Shaleev, M., Petrov, M., Schilling, J., 2017. Quantum dot emission driven by mie resonances in silicon nanostructures. Nano Lett. 17 (11), 6886–6892. https://doi.org/10.1021/acs.nanolett.7b03248.

Sauvan, C., Hugonin, J.P., Maksymov, I.S., Lalanne, P., 2013. Theory of the spontaneous optical emission of nanosize photonic and plasmon resonators. Phys. Rev. Lett. 110, 1–5. https://doi.org/10.1103/PhysRevLett.110.237401.

Savasta, S., Saija, R., Ridolfo, A., Di Stefano, O., Denti, P., Borghese, F., 2010. Nanopolaritons: Vacuum rabi splitting with a single quantum dot in the center of a dimer nanoantenna. ACS Nano 4, 6369–6376. https://doi.org/10.1021/nn100585h.

Schuller, J.A., Brongersma, M.L., 2009. General properties of dielectric optical antennas. Opt. Express. 17, 24084. https://doi.org/10.1364/OE.17.024084.

Sevgi, L., ed., 2014. Finite-Difference Time-Domain Method, in: Electromagn. Model. Simul., John Wiley & Sons, Inc., Hoboken, NJ, USA, pp. 407–513. 10.1002/9781118716410.ch14.

Shcherbakov, M.R., Neshev, D.N., Hopkins, B., Shorokhov, A.S., Staude, I., Melik-Gaykazyan, E.V., Decker, M., Ezhov, A.A., Miroshnichenko, A.E., Brener, I., Fedyanin, A.A., Kivshar, Y.S., 2014. Enhanced third-harmonic generation in silicon nanoparticles driven by magnetic response. Nano Lett. 14 (11), 6488–6492. https://doi.org/10.1021/nl503029j.

Shibanuma, T., Albella, P., Maier, S.A., 2016. Unidirectional light scattering with high efficiency at optical frequencies based on low-loss dielectric nanoantennas. Nanoscale 8 (29), 14184–14192. https://doi.org/10.1039/C6NR04335F.

Sikdar, D., Cheng, W., Premaratne, M., 2015. Optically resonant magneto-electric cubic nanoantennas for ultra-directional light scattering. J. Appl. Phys. 117, 83101. https://doi.org/10.1063/1.4907536.

Sinev, Ivan et al, 2020. Steering of Guided Light with Dielectric Nanoantennas. ACS Photonics 7 (3), 680–686. https://doi.org/10.1021/acsphotonics.9b01515.

Sortino, L., Zotev, P.G., Mignuzzi, S., Cambiasso, J., Schmidt, D., Genco, A., Aßmann, M., Bayer, M., Maier, S.A., Sapienza, R., Tartakovskii, A.I., 2019. Enhanced light-matter interaction in an atomically thin semiconductor coupled with dielectric nano-antennas. Nat. Commun. 10, 1–8. https://doi.org/10.1038/s41467-019-12963-3.

Staude, I., Miroshnichenko, A.E., Decker, M., Fofang, N.T., Liu, S., Gonzales, E., Dominguez, J., Luk, T.S., Neshev, D.N., Brener, I., Kivshar, Y., 2013. Tailoring directional scattering through magnetic and electric resonances in subwavelength silicon. ACS Nano 7, 7824–7832.

Staude, I., Khardikov, V.V., Fofang, N.T., Liu, S., Neshev, D.N., Luk, T.S., Brener, I., Kivshar, Y.S., 2015. Shaping photoluminescence spectra with magnetoelectric resonances in all-dielectric nanoparticles. ACS Photonics. https://doi.org/10.1021/ph500379p.

Sugimoto, H., Fujii, M., 2017. Colloidal dispersion of subquarter micrometer silicon spheres for low-loss antenna in visible regime. Adv. Opt. Mater. 5, 1700332. https://doi.org/10.1002/adom.201700332.

Taminiau, T.H., Stefani, F.D., van Hulst, N.F., 2008. Enhanced directional excitation and emission of single emitters by a nano-optical Yagi-Uda antenna. Opt. Express. 16, 10858. https://doi.org/10.1364/oe.16.010858.

Tian, J., Li, Q., Yang, Y., Qiu, M., 2016. Tailoring unidirectional angular radiation through multipolar interference in a single-element subwavelength all-dielectric stair-like nanoantenna. Nanoscale 8 (7), 4047–4053. https://doi.org/10.1039/C5NR06964E.

Tiguntseva, E.Y., Zograf, G.P., Komissarenko, F.E., Zuev, D.A., Zakhidov, A.A., Makarov, S.V., Kivshar, Y.S., 2018. Light-emitting halide perovskite nanoantennas. Nano Lett. 18 (2), 1185–1190. https://doi.org/10.1021/acs.nanolett.7b04727.

Timpu, F., Sergeyev, A., Hendricks, N.R., Grange, R., 2017. Second-harmonic enhancement with mie resonances in perovskite nanoparticles. ACS Photonics 4 (1), 76–84. https://doi.org/10.1021/acsphotonics.6b00570.

Törmä, P., Barnes, W.L., 2015. Strong coupling between surface plasmon polaritons and emitters: a review. Reports Prog. Phys. 78 (1), 013901. https://doi.org/10.1088/0034-4885/78/1/013901.

Tribelsky, M.I., Geffrin, J.M., Litman, A., Eyraud, C., Moreno, F., 2016. Directional Fano resonances in light scattering by a high refractive index dielectric sphere. Phys. Rev. B. 94,. https://doi.org/10.1103/PhysRevB.94.121110 121110.

van de Haar, M.A., van de Groep, J., Brenny, B.J.M., Polman, A., 2016. Controlling magnetic and electric dipole modes in hollow silicon nanocylinders. Opt. Express. 24, 2047. https://doi.org/10.1364/oe.24.002047.

Vaskin, A., Bohn, J., Chong, K.E., Bucher, T., Zilk, M., Choi, D.-Y., Neshev, D.N., Kivshar, Y.S., Pertsch, T., Staude, I., 2018. Directional and spectral shaping of light emission with mie-resonant silicon nanoantenna arrays. ACS Photonics 5 (4), 1359–1364. https://doi.org/10.1021/acsphotonics.7b01375.

Wang, Z., An, N., Shen, F., Zhou, H., Sun, Y., Jiang, Z., Han, Y., Li, Y., Guo, Z., 2017. Enhanced forward scattering of ellipsoidal dielectric nanoparticles. Nanoscale Res. Lett. 12, 58. https://doi.org/10.1186/s11671-016-1794-x.

Wang, Z.Y., Zhang, R.J., Wang, S.Y., Lu, M., Chen, X., Zheng, Y.X., Chen, L.Y., Ye, Z., Wang, C.Z., Ho, K.M., 2015. Broadband optical absorption by tunable Mie resonances in silicon nanocone arrays. Sci. Rep. 5, 1–6. https://doi.org/10.1038/srep07810.

Wiecha, P.R., Cuche, A., Arbouet, A., Girard, C., Colas des Francs, G., Lecestre, A., Larrieu, G., Fournel, F., Larrey, V., Baron, T., Paillard, V., 2017. Strongly directional scattering from dielectric nanowires. ACS Photonics 4 (8), 2036–2046. https://doi.org/10.1021/acsphotonics.7b00423.

Wu, X., Gray, S.K., Pelton, M., 2010. Quantum-dot-induced transparency in a nanoscale plasmonic resonator. Opt. Express. 18, 23633. https://doi.org/10.1364/oe.18.023633.

Yan, Y., Zeng, Y., Wu, Y., Zhao, Y., Ji, L., Jiang, Y., Li, L., 2014. Ten-fold enhancement of ZnO thin film ultraviolet-luminescence by dielectric microsphere arrays. Opt. Express. 22, 23552. https://doi.org/10.1364/oe.22.023552.

Yao, K., Liu, Y., 2016. Controlling electric and magnetic resonances for ultracompact nanoantennas with tunable directionality. ACS Photonics 3 (6), 953–963. https://doi.org/10.1021/acsphotonics.5b00697.

Yavas, O., Svedendahl, M., Dobosz, P., Sanz, V., Quidant, R., 2017. On-a-chip biosensing based on all-dielectric nanoresonators. Nano Lett. 17 (7), 4421–4426. https://doi.org/10.1021/acs.nanolett.7b0151810.1021/acs.nanolett.7b01518.s001.

Yu, F., Persson, B., LöfÔs, S., Knoll, W., 2004. Surface plasmon fluorescence immunoassay of free prostate-specific antigen in human plasma at the femtomolar level. Anal. Chem. 76 (22), 6765–6770. https://doi.org/10.1021/ac048937w10.1021/ac048937w.s001.

Yuan, S., Qiu, X., Cui, C., Zhu, L., Wang, Y., Li, Y., Song, J., Huang, Q., Xia, J., 2017. Strong photoluminescence enhancement in all-dielectric fano metasurface with high quality factor. ACS Nano 11 (11), 10704–10711. https://doi.org/10.1021/acsnano.7b04810.

Zakharko, Y., Graf, A., Schießl, S.P., Hähnlein, B., Pezoldt, J., Gather, M.C., Zaumseil, J., 2016. Broadband tunable, polarization-selective and directional emission of (6,5) carbon nanotubes coupled to plasmonic crystals. Nano Lett. 16 (5), 3278–3284. https://doi.org/10.1021/acs.nanolett.6b00827.

Zhang, J., MacDonald, K.F., Zheludev, N.I., 2013. Near-infrared trapped mode magnetic resonance in an all-dielectric metamaterial. Opt. Express. 21, 26721. https://doi.org/10.1364/oe.21.026721.

Zhang, Y., Nieto-Vesperinas, M., Sáenz, J.J., 2015. Dielectric spheres with maximum forward scattering and zero backscattering: a search for their material composition. J. Opt. (United Kingdom) 17,. https://doi.org/10.1088/2040-8978/17/10/105612 105612.

Zhao, J., Wu, L., Zhi, J., 2008. Fabrication of micropatterned ZnO/SiO2 core/shell nanorod arrays on a nanocrystalline diamond film and their application to DNA hybridization detection. J. Mater. Chem. 18, 2459–2465. https://doi.org/10.1039/b800029h.